

Article

Neutral Beam Coupling with Plasma in a Compact Fusion Neutron Source

Eugenia Dlougach ^{1,*}, Alexander Panasenkov ¹, Boris Kuteev ¹ and Arkady Serikov ^{2,*}¹ NRC Kurchatov Institute, 123182 Moscow, Russia² Karlsruhe Institute of Technology (KIT), Institute for Neutron Physics and Reactor Technology, Hermann-von-Helmholtz-Platz 1, 76344 Eggenstein-Leopoldshafen, Germany

* Correspondence: edlougach@gmail.com (E.D.); arkady.serikov@kit.edu (A.S.)

Featured Application: The “*Lite Neutral Beam*” model (LNB) efficiently combines an injected beam detailed description with data processing pipeline for following up particle statistics. This approach allows one to study the issues of beam-plasma interaction in fusion devices and to perform on-the-fly optimization of beam-driven toroidal systems. The results are important for a steady-state current drive and fusion controllability in low aspect ratio and spherical tokamaks; they are also applicable to a conventional tokamak design.

Abstract: FNS-ST is a fusion neutron source project based on a spherical tokamak ($R/a = 0.5 \text{ m}/0.3 \text{ m}$) with a steady-state neutron generation of $\sim 10^{18} \text{ n/s}$. Neutral beam injection (NBI) is supposed to maintain steady-state operation, non-inductive current drive and neutron production in FNS-ST plasma. In a low aspect ratio device, the toroidal magnetic field shape is not optimal for fast ions confinement in plasma, and the toroidal effects are more pronounced compared to the conventional tokamak design (with $R/a > 2.5$). The neutral beam production and the tokamak plasma response to NBI were efficiently modeled by a specialized beam-plasma software package BTR-BTOR, which allowed fast optimization of the neutral beam transport and evolution within the injector unit, as well as the parametric study of NBI induced effects in plasma. The “*Lite neutral beam model*” (LNB) implements a statistical beam description in 6-dimensional phase space ($10^6\text{--}10^{10}$ particles), and the beam particle conversions are organized as a data flow pipeline. This parametric study of FNS-ST tokamak is focused on the beam-plasma coupling issue. The main result of the study is a method to achieve steady-state current drive and fusion controllability in beam-driven toroidal plasmas. LNB methods can be also applied to NBI design for conventional tokamaks.



Citation: Dlougach, E.; Panasenkov, A.; Kuteev, B.; Serikov, A. Neutral Beam Coupling with Plasma in a Compact Fusion Neutron Source. *Appl. Sci.* **2022**, *12*, 8404. <https://doi.org/10.3390/app12178404>

Academic Editor: Emilio Martines

Received: 8 July 2022

Accepted: 15 August 2022

Published: 23 August 2022

Publisher’s Note: MDPI stays neutral with regard to jurisdictional claims in published maps and institutional affiliations.



Copyright: © 2022 by the authors. Licensee MDPI, Basel, Switzerland. This article is an open access article distributed under the terms and conditions of the Creative Commons Attribution (CC BY) license (<https://creativecommons.org/licenses/by/4.0/>).

1. Introduction

Spherical tokamaks (ST) can provide high neutron flux density and good compatibility with fission blankets at a lower cost than conventional tokamaks. A neutron source FNS-ST with a compact design based on a spherical tokamak [1] is expected to provide a stationary neutron flux of $\sim 10^{18} \text{ n/s}$. The device operating parameters ($T_e = 5 \text{ keV}$, $n_e = 10^{20} \text{ m}^{-3}$) are chosen accounting for a high neutral beam (NB) contribution to non-inductive current drive (CD). The estimated NB contribution to neutron yield is up to 99%, coming from deuterium-tritium (DT) fusion between hot beam particles and relatively cold plasma, with a Maxwell velocity distribution [2]. NB tangential injection is also an efficient current driver, since the fast ions produced and captured by plasma create a current parallel to the magnetic field during their circulation and deceleration (slowing down) in the plasma. The beam ion current, together with the bootstrap current fully substitutes the inductive current in FNS-ST plasma, ensuring the steady-state operation of the device [3]. However,

additional heating and CD systems significantly increase the cost of the entire machine. In addition, due to the low aspect ratio (R/a) and moderate values of the toroidal magnetic field, the relative fraction of fast particle losses in a spherical tokamak significantly exceeds that in tokamaks with a high aspect ratio (classical or conventional) [4], since the Larmor radius of fast ions at the low field side of torus can be comparable with a rather low minor radius, and with the magnetic field variation scale. In order to minimize the losses of fast particles and to boost the injected power, the parameters of NB injection need to be chosen accounting for the beam efficient penetration to plasma, and to ensure the most favorable beam deposition within the plasma core volume.

For an efficient neutral beam current drive (NB^{CD}), the beam energy should exceed by a factor of 3–5 [5] the so-called critical energy [6], the latter depends on the plasma electron temperature and on the normalized beam mass (i.e., the ratio of the beam to the background ion mass). NB^{CD} increases with higher electron temperature and lower plasma density, which extend the fast ion thermalization time. Taking into account the toroidal geometry and the strong inhomogeneity of parameters across plasma cross section, all the beam-driven effects, including NB^{CD}, beam-plasma fusion rates, heating and plasma rotation, are sensitive to instant fast ions (FI) deposition in plasma. The FI spatial distribution produced by the beam, or NB footprint, is defined by the beam atom penetration depth in plasma, or rather, the average path of individual groups of fast atoms before their ionization point. As a result, factors such as beam penetration depth, FI circulation time, and direct losses of fast atoms and released ions, finally determine the choice of the beam-plasma mode operation and NB aiming tuning in a beam-driven tokamak.

The problem of geometry impact on beam-plasma interaction is highlighted in [7], where different calculation models of NBI are compared, and the results show a visible discrepancy in the fast ion distribution and loss of NB performance between various beam models applied to the same beam-plasma system. In addition, the experimental data, which are not in a perfect agreement with NB^{CD} simulation, especially for off-axis tangential injection [8,9], also motivated us to perform a more detailed study of beam-plasma geometry impact on NB efficiency.

The beam spatial shape and angular distribution (6-dimensional NB geometry in a phase space) have an essential impact on the beam ions release in plasma and their final capture by the magnetic field. The release point radius and initial pitch angle (the angle between the ion velocity and the magnetic field vector) of the fast particles result in a wide scattering across the beam constituent rays, which can lead to a lower FI fraction captured to the most favorable magnetic orbits, with higher CD efficiency and neutron output. The overall performance of a *thick* (realistic) NB shape is essentially lower compared to classical *thin* beam models (e.g., traditional pencil-like representation [10]).

In compact tokamak devices, including spherical design, the size of the beam envelope cross section can be of the same order as the plasma cross section, so the shaping effects are generally more pronounced. The enhanced orbital losses stem from the combination of the beam ions statistics in 6-dimensional phase space and the magnetic field topology. It is important to add that NBI optimum operating range is predominantly based on currently available and cost-effective neutral beam production technologies. The NB composition and spectra are commonly defined by the NB creation scheme.

Several efficient NBI models and codes have been presented recently, which are capable to calculate NBI fast ion distribution almost in real time, due to simplified fast ion birth procedure, very low ion orbits statistics for interpolation, and analytical solution of the Fokker-Planck equation, e.g., as implemented in RABBIT code [11]. To speed up the calculation, the effect of beam shaping is included analytically. The RABBIT code is reported to run ~1000 times faster compared with NUBEAM code [12], showing small deviations (~10%) between the results, which is supposed to be acceptable for many applications. However, a more sophisticated approach of beam geometry representation [13] has proved to offer a more reliable and accurate NBI simulation, especially for studying three-dimensional beam-plasma phenomena. Finally, in the context of integrated tokamak

modelling frameworks, there are NBI models based on simplified (narrow-beam) approach, with generalization to a realistic NBI geometry, e.g., NEMO code [14]. The main advantage of the mixed approach is its modularity, with the possibility to work with any tokamak equilibrium and injector geometry; it can also be integrated in a workflow with any global transport code.

To study the geometry impact on NB response and performance in tokamak plasmas, we propose a light-weighted technique of multi-ray beam tracing (LNB, Lite Neutral Beam) [15], which strikes a balance between the best features of the present-day advanced NBI models, i.e., high accuracy, flexibility, almost real-time performance, and finally the ability to be integrated in a calculation workflow.

The LNB approach is generalized in a software package BTR-BTOR. The beam statistics are normally represented by 10^5 – 10^9 particles derived from BTR code [16,17]. BTR code was developed 25 years ago to target the issues of NBI design [18], and has been actively used since 2005 until now, especially in ITER NBI design and study [19]. In BTOR pipeline (Beam in TORoids) [20], the numerical methods for particle tracing and transformations, as well as the input beam model itself are inherited from BTR code. The numerical procedures are deterministic and easy tractable, all the results can be reproduced and easily explained. The BTOR code takes the BTR data set containing the detailed NB atoms statistics, composed of phase coordinates and current fraction, and next, “propagates” the beam data flow through tokamak plasma: through the beam ionization, and the slowing down until relaxation. This approach allows for calculation of particle distributions in the phase space, beam losses estimation, NB heating efficiency, NBCD, beam-plasma fusion rates, and other beam induced effects. The main idea of BTR-BTOR workflow was to apply a highly efficient BTR technique to all beam-driven events, i.e., to the source beam simulation, atom ionization, fast ion slowing down and fusion probability calculation. All the numerical models used are straight-forward and optimized for performance, so the BTOR approach is suitable for fast parametric studies of beam-plasma operation scenarios, including sensitivity analysis.

The paper introduces the LNB approach implemented in the BTOR v.1 software pipeline and demonstrates its capabilities when applied to the analysis of NBI losses and performance in a compact neutron source FNS-ST. The requirements for NBI scheme selection for FNS-ST tokamak, and the NB internal structure, processed by BTR code, are represented in Section 2. BTOR software package and numerical methods are described in Section 3. NB penetration and fast ion deposition in plasma are discussed in Section 4. NB shine-through losses are evaluated in Section 5. Fast ions losses and toroidal magnetic field effects are estimated in Section 6. Fast ion distributions in energy space are considered in Section 7. The NB current drive and the neutron generation are treated in Section 8. The optimum NB parameters for FNS-ST are suggested in Section 9. The main conclusions are made in Conclusions and Outlook (Section 10).

2. NBI Scheme for FNS-ST and the Source Beam Structure

2.1. FNS-ST Purpose and NBI Requirements

The NBI system for FNS-ST is designed to deliver a steady-state beam power about 6–10 MW in total. According to the design, NBI consists of four injector units, each unit delivers ~ 3.3 MW atomic power to FNS-ST plasma, formed by deuterium and tritium ions with approximate ratio 0.5/0.5. The nominal beam port size is currently $0.3 \times 0.6 \text{ m}^2$, although a reduction to $0.1 \times 0.3 \text{ m}^2$ is very desirable. The injection axis can be either steered horizontally, or inclined, while the tangential injection radius range is: $R_{\text{inj}} = 0.4$ – 0.6 m. The main parameters of the machine are summarized in Table 1.

Table 1. FNS-ST tokamak design parameters.

| Parameter | Value/Range |
|---|---------------------------------------|
| Aspect ratio R/a , m/m | 0.5/0.3 |
| Elliptic elongation k | ~3 (2.75) |
| Toroidal magnetic field, T | 1.5 |
| Electron temperature T_e , keV | 1–5 |
| Average plasma density n_e , 10^{20} m^{-3} | 0.5–1 |
| Plasma current I_p , MA | 0.8–1.5 |
| NB tangential injectors number | 3–4 |
| NB total power P_b , MW | 6–10 |
| NB port size $W \times H$, m ² | 0.3×0.6 (0.1×0.3) |
| D^0/T^0 atoms energy, keV | 100–200 |
| Ion source current, A | 80 |
| NB injection current $I_{0\text{inj}}$, A | 30–40 |
| Axis inclination angle, degree | 0–30 |

2.2. NBI Options and Preferences

The choice of NB production technology and the beamline design depends on the energy range of the particles that can be transmitted to plasma, ensuring the efficient CD and neutron yield. The injected beam energy should be also consistent with the beam species mass (e.g., hydrogen, deuterium, or tritium), and with the plasma content. The cross-section of beam particle ionization in plasma depends on its relative velocity over the target plasma species. It naturally implies similar beam ionization profiles for different hydrogen isotopes when their energy ratio corresponds to their mass ratio.

The atomic beam is produced by extraction of ions, their acceleration to high energy and neutralization on a gas target, while other neutralization techniques are still not elaborated enough to be widely applied. Depending on the required beam energy, there are two possible design solutions for NBI [21]. For energies below 75 keV/nucleon (150 keV in deuterium), a positive ion-based technique is more efficient, while for higher beam energies, negative ion-based solutions are preferable. The neutralization yield per ion current normalized to a source current of 1 A in the “positive” scheme decreases rapidly with energy, so NB production with $E_b > 75$ keV/nucleon from positive ions is associated with high power losses (~70% of ions to waste), although this energy level is better for tangential beam penetration into FNS-ST dense plasma (densities $n_e \sim 1 \cdot 10^{20} \text{ m}^{-3}$). An alternative injector scheme based on negative ions is more attractive for the energy range 100–500 keV/nucleon, with high neutral yield (~60%), which is almost independent of the ion energy. “Negative” beamlines are more efficient in beam transmission to plasma, since a negative ion beam has lower angular dispersion compared to a positive ion beam. However, the positive ion current density is significantly higher than the current density achieved for negative ion sources, so the positive beamline design is typically much more compact, the injector technology is better understood and widely implemented, and the positive ion scheme is preferential even for the beam energy falling within the “transition” range $E_b = 75–100$ keV/nucleon (where the neutralization efficiency drops to 20–30%).

A detailed NBI design schemes comparison for FNS-ST [21] resulted in the following conclusions:

- Regardless of the beamline design, the injector chamber should be mounted without inclination, i.e., horizontally, since the mass of the chamber with the beamline components is dozens of tons, and their installation on an inclined platform with proper adjustment with further remote maintenance is almost impossible.

- The “negative” scheme has a high efficiency in power, which is practically independent of the beam energy. The efficiency of beam transmission (for nominal NBI port dimensions) is high enough; for residual ions deflection and dumping (RID), and the negative scheme applies an electrostatic device (ERID) of fairly compact size.
- The NBI negative scheme weak points included a low current density extracted from the ion source ($\sim 20 \text{ mA/cm}^2$), a “halo” fraction ($\sim 15\%$) with higher angular spread which accompanies the beam core current and thus is fully intercepted by the beamline components, and plasma emitter non-uniformity across large surface of ion source, which can affect the overall beam transmission. A negative scheme is supposed to be more efficient for NBI energy $E_b > 75 \text{ keV/nucleon}$.
- A positive beamline is preferential for NBI energy $E_b < 75 \text{ keV/nucleon}$. A higher current density (200 mA/cm^2) is extracted from the beam source and thus lowers the emitter area required. A compact neutralizer can be attached directly to the ion source exit, which leads to lower gas flows and moderate cryopanels loading. Positive scheme NBI performance in power is almost a half of the negative scheme. Additionally, the positive ion source beam composition includes molecular ion fractions, which produce lower energy atoms in dissociation and neutralization (i.e., $E_b/2$ and $E_b/3$). These ion fractions are captured by the periphery tokamak plasma and merely drop out from current drive and neutron generation. We also note, that in a positive beamline scheme, the beam current density and volume charge are high enough, so electrostatic RID cannot be applied. Instead, a massive magnetic ion dump is used, with a large panel size capable of intercepting all the energy fractions of residual ions. For $E_b \sim 140 \text{ keV}$, the residual ion power can be twice as high as the effective beam power in neutrals, so the magnetic RID appears to be the most power loaded component of the beamline.

The injection port size forms a major restriction for NB power input, especially for a small tokamak operating at high neutron flux from the plasma core. The port minimum size is designed accounting for the ion source current density, the expected angular width and beam focusing methods. The design solutions also depend on the power load study for all the beamline surfaces due to beam direct interception and re-ionization, and the loads should be within the heat removal constraints along the beam ducts region. Both beamline schemes (positive and negative) were considered for the window port size justification [21] in FNS-ST tokamak. A parametric analysis of the beam power losses resulted in an injection port size ($W \times H$) of $30 \times 60 \text{ cm}^2$, when almost 80% of NB power is transmitted to plasma, in case of optimum (ideal) beam focusing. Since this port size is equal to the plasma minor radius (0.3 m), its reduction, at least down to $0.2 \times 0.4 \text{ m}^2$, is also discussed.

As a result, for the NB injection to FNS-ST plasma, with a required neutral power range of 6–10 MW, well-developed beamline technology based on positive ions was chosen as the preferred solution [21]. The NBI design consists of four injector units. Three units are in operation, one is for maintenance and regeneration, and each injection unit delivers 2–3.5 MW to plasma in deuterium atoms with an energy of $E_b = 100\text{--}140 \text{ keV}$. The NBI unit layout is shown in Figure 1.

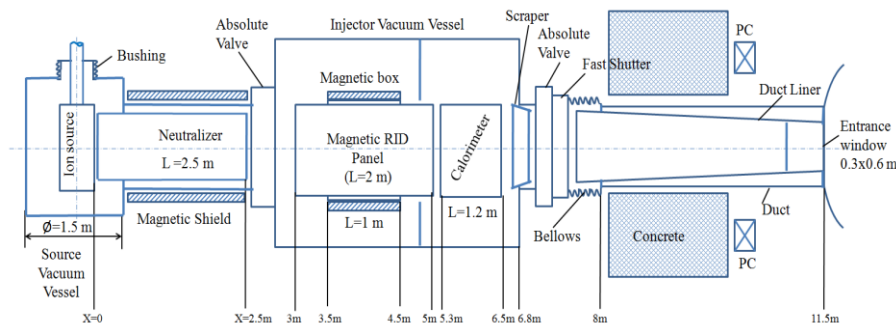


Figure 1. FNS-ST neutral beam injector setup with D+ ion source (taken from [21]).

The main components of each NBI unit are:

- A positive ion source-accelerator (ISA), with a plasma emitter area of $18 \times 115 \text{ cm}^2$ and a four-grids ion-optical acceleration system. Each grid consists of five sections, with 80 beam apertures. The source beam structure and focusing are discussed below in more detail, while the beam design is shown in Figure 2 (BTR screen);
- A neutralizer is attached to the ISA exit with a channel cross-section $18 \times 120 \text{ cm}$ for beam passage, and is filled with D_2 gas (neutralization target);
- An absolute vacuum valve (AVV) is located at the entrance to the injector vacuum vessel (VV);
- A compact magneto-static residual ion deflector (MRID) deflects the ions horizontally to the side panel, which is capable of accepting a high load of up to 5.5 MW with peak power density values of up to 14 MW/m^2 and to intercept all the ion energy fractions. Magnetic deflection is performed within an electromagnetic steel box with opposite windings, so that in the beam passage area the magnetic field is almost uniform;
- A calorimeter, or NB dump is for beam interception during the ISA training, diagnostics and injector adjustment, i.e., before the actual beam injection starts;
- After the VV, the beam passes through the duct, with a water-cooled liner inserted to remove the beam power (including scraped atoms and re-ionized flux deflected in the stray magnetic field). At the VV exit, before the duct, a scraper device is installed, to cut the beam angular “tail” and reduce the power load onto the connecting duct elements.

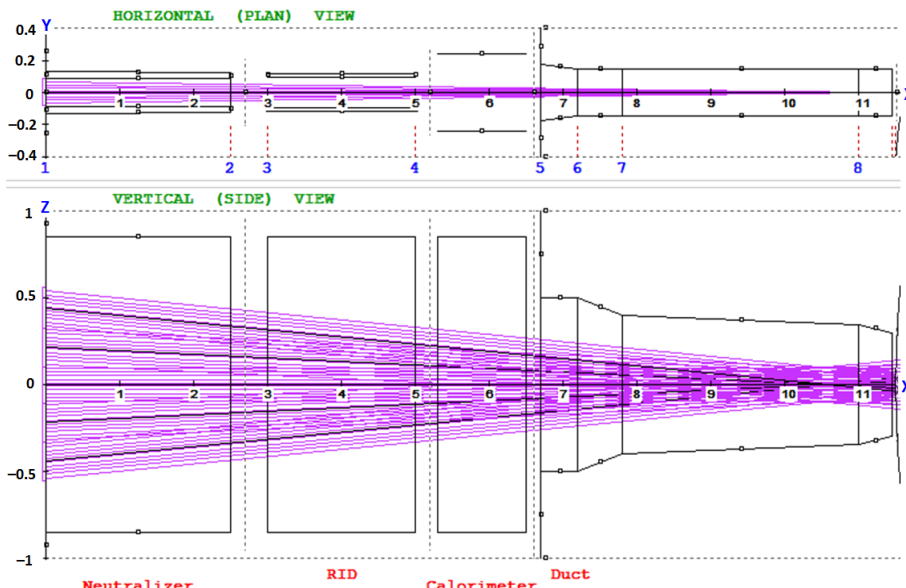


Figure 2. FNS-ST NBI beamlets axes focusing (BTR main screen).

2.3. Neutral Beam Structure

The shape of the beam and its internal structure are determined by beamlet focusing provided by the ion-optical system (IOS) and by the beamlets’ internal angular dispersion. The ion beam, initially formed by the plasma emitter and accelerated in a multi-grid multi-aperture IOS, consists of 400 beamlets in accordance with the apertures setup across the extraction and acceleration grids (electrodes). In the FNS-ST injector unit based on positive ions, the source beam is organized as a vertical column of five rectangular sections (beamlet clusters) with 80 beamlets each. To ensure efficient beam transmission to the tokamak without overheating the beamline elements, the beamlet focusing is rather complex. All the beamlets throughout the IOS column in a horizontal plane are aimed at NBI port center-point, while in a vertical plane, within each cluster, the beamlets axes are parallel to the cluster axis, and the clusters’ axes are steered to reduce the entire beam cross-section at NBI port plane in tokamak. The beamlet focusing scheme is shown in Figure 2.

The ion current within each beamlet is supposed to have a normal distribution along the polar angle, and the sum of Gaussian fractions fits the beam angular shape in all NBI schemes. For example, the positive ion beam in FNS-ST is well matched by a two-dimensional Gaussian profile (with different standard deviations along horizontal and vertical axes), while a negative ion beam, combined by two angular fractions (core and halo) can be reproduced by a sum of one-dimensional profiles versus polar angle from the beamlet axis:

$$j(\theta) = \frac{1-H}{\pi\Delta_c^2}e^{-\theta^2/\Delta_c^2} + \frac{H}{\pi\Delta_h^2}e^{-\theta^2/\Delta_h^2}, \quad (1)$$

where θ is a polar angle from the beamlet axis, H is so called halo fraction, and Δ_c and Δ_h are the angular widths of the core and halo. Note that the Gaussian width in our notation is not the same as the standard deviation σ for normal distribution. The positive ion beam in FNS-ST is supposed to carry a single core fraction, with no halo.

The positive ion beamlet angular width in the FNS-ST NBI is assumed to be 15 mrad, which implies that at a distance of 11.5 m, i.e., at the NB port plane, each beamlet footprint is ~33 cm in diameter; therefore, the nominal NB port width was chosen to be 30 cm. With the beamlets perfect alignment towards the center-point of the $30 \times 60 \text{ cm}^2$ NBI window, the calculated beam transmission efficiency is ~76%, with an injected power of 3.5 MW. If the beamlets' alignment is not perfect (the beam is "misaligned"), with errors of ± 4 mrad in the horizontal and ± 6 mrad in the vertical direction, the NB power delivered to plasma reduces down to 3.3 MW (with the beam transmission ~71%), as shown in Figure 3.

Since a reduced size of the injection port is highly preferred, an option of NB injection through a window size $20 \times 40 \text{ cm}^2$ was considered and compared with the window nominal size $30 \times 60 \text{ cm}^2$. The result profiles of beam power delivered are shown in Figure 4. With perfect beam alignment to the $20 \times 40 \text{ cm}^2$ injection port center-point, the calculated beam transmission was ~50%, with an injection power of ~2.3 MW, which corresponds to a one third decrease from the nominal case. With misalignment of $4/-6$ mrad along horizontal/vertical axes, the power input to the plasma reduces down to 2.1 MW (reduced 36% from the nominal port size, with NB transmission decay down 46%). Taking into account the neutralization yield $< 50\%$, the overall NBI performance was about 25%, and all the injector units delivered only ~6 MW to FNS-ST plasma. The reduced port size augmented the power load faced by the beamline elements, which makes the adopted heat removal approach not applicable; hence, an entire NBI design revision will be required if the NBI port size is reduced.

Finally, the influence of horizontal beamlet focusing on beam transmission was studied. Instead of the nominal case of beamlets horizontal focusing, the simplified beam geometry with parallel beamlets in the horizontal plane was considered. However, in this variant, the vertical focusing of the beam clusters on the center of the NB port was preserved. The result was not quite evident. The beam transmission was reduced slightly, from 50% to 48% for perfect alignment, and from 46% to 43% for a nominal deviation of $4/-6$ mrad. The beam power profiles obtained at the NBI port plane for a $20 \times 40 \text{ cm}^2$ opening are shown in Figure 5.

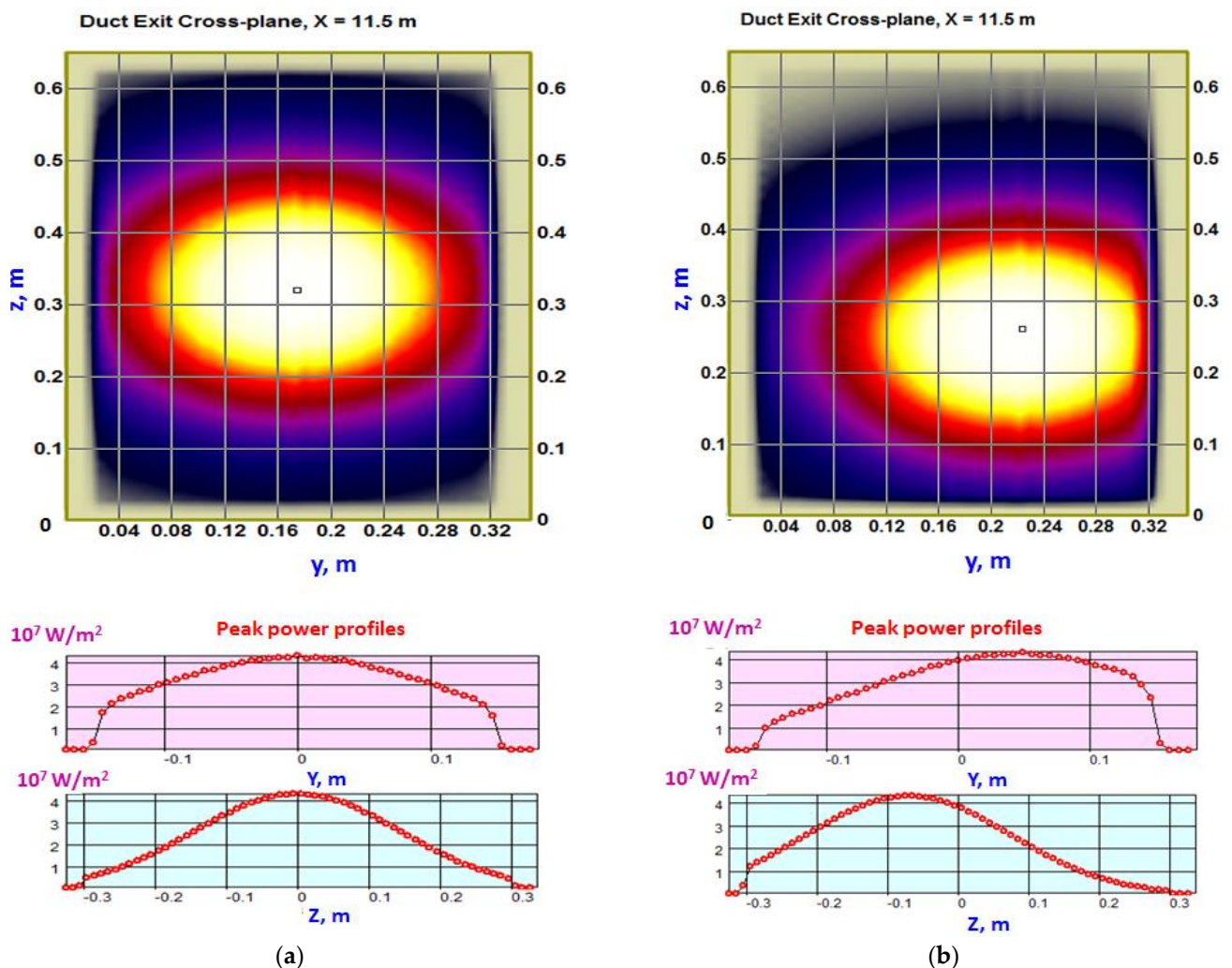


Figure 3. Power density maps (in BTR color maps maximum density is shown white, minimum non-zero is black, zero load is olive-colored), and peak profiles of the neutral beam, which is injected to the FNS-ST plasma through an NBI port with a size of $30 \times 60 \text{ cm}^2$. All beamlets are focused in horizontal plane at 10.5 m: (a) ideal alignment, total power—3.49 MW, peak density— 43.3 MW/m^2 ; (b) beam misalignment 4°–6 mrad, total power—3.27 MW, peak density— 43.1 MW/m^2 . BTR maps are shown in local coordinates, the map aspect ratio is changed to fit the screen space; for BTR power density profiles, the axes X, Y and Z correspond to NBI coordinates shown in Figure 2.

Beam particle distributions (phase diagrams) in a four-dimensional space across the beam axis (X, Y, θ_x , and θ_y) are shown in Figures 6 and 7 for the IOS exit plane and for the NBI port plane (window size $30 \times 60 \text{ cm}^2$). The statistics on beam source ion population were provided by BTR code, which also calculates the source beam neutralization and follows the atoms through the total beamline and ducts accounting for direct and re-ionized beam losses. Beam statistics at the tokamak NB port plane (Figure 7) were applied to trace the beam particles ensemble in the tokamak plasma until relaxation. For this purpose, the BTOR software was developed to accept the injected beam statistics, calculate the ionization of the fast beam atoms, evaluate ion population losses and capture by magnetic field, and follow up fast ion deceleration to thermal velocities. Fast and simple BTOR methods allowed efficient simulation of the beam-driven effects, among which are the beam current drive, the beam-plasma fusion, plasma heating and rotation. The calculation models and results are presented in the following sections.

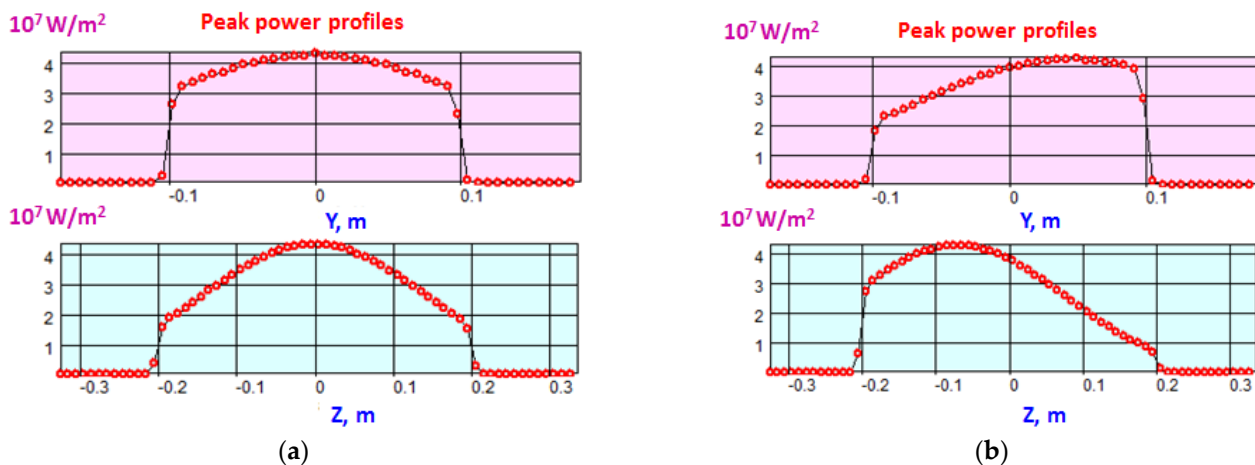


Figure 4. Power density profiles of the neutral beam injected to the FNS-ST plasma through NBI port with a size of $20 \times 40 \text{ cm}^2$. The beamlets are focused in a horizontal plane at 10.5 m. (a) Ideal alignment, total power—2.31 MW, peak density— 43.3 MW/m^2 ; (b) beam misalignment 4/-6 mrad, total power—2.06 MW, peak density— 43.1 MW/m^2 . For BTR power density profiles, the axes X, Y and Z correspond to NBI coordinates shown in Figure 2.

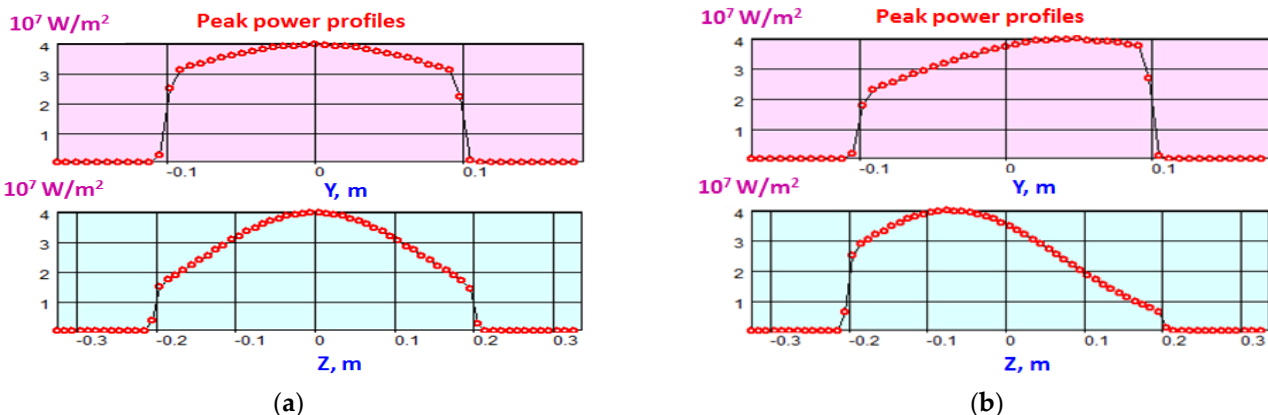


Figure 5. Power density profiles of the neutral beam injected to the FNS-ST plasma through NBI port with a size of $20 \times 40 \text{ cm}^2$ with parallel beamlets. (a) Ideal alignment, total power—2.19 MW, peak density— 39.99 MW/m^2 ; (b) beam misalignment 4/-6 mrad, total power—1.96 MW, peak density— 40.1 MW/m^2 . For BTR power density profiles, the axes X, Y and Z correspond to NBI coordinates shown in Figure 2.

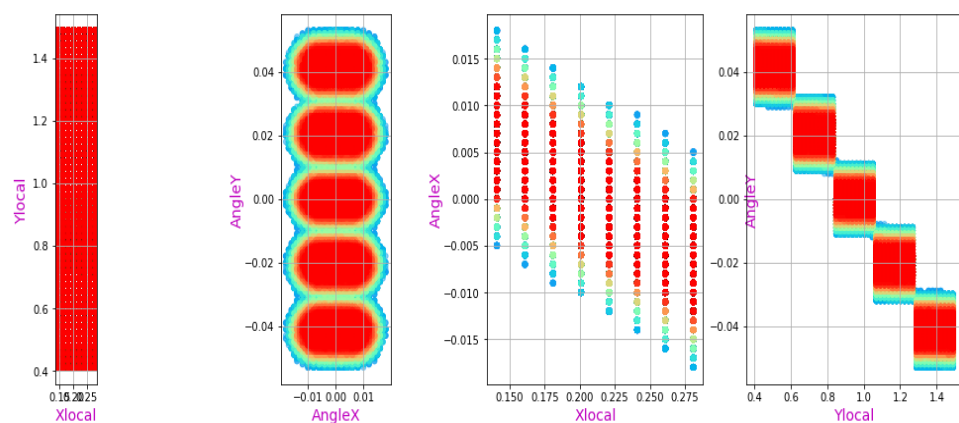


Figure 6. Beam source particles statistical distribution before neutralization, left to right: (X, Y) , (θ_x, θ_y) , (X, θ_x) , (Y, θ_y) , where X , Y —horizontal and vertical position in the plane, θ_x , θ_y —horizontal and vertical angle from the beam main axis. The beam source spatial dimensions (shown in the left plot) correspond to the plasma emitter rectangle $W \times H = 18 \times 115 \text{ cm}^2$.

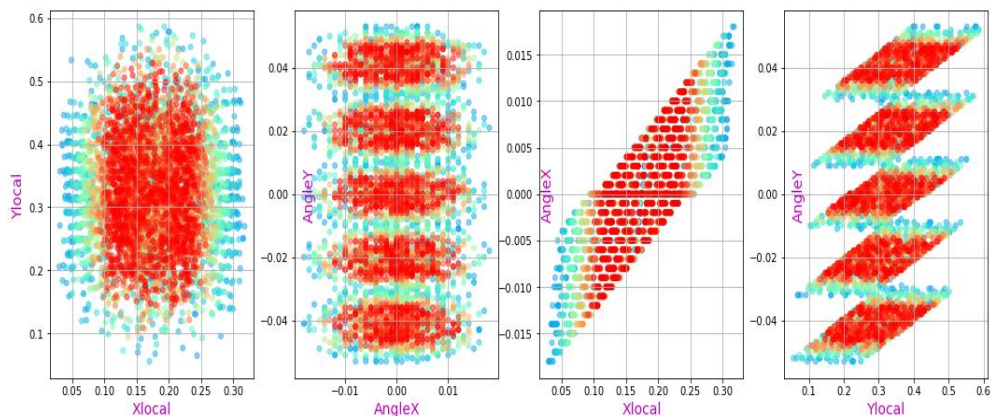


Figure 7. Neutral beam distribution in the NBI port plane: (X, Y) , (θ_x, θ_y) , (X, θ_x) , (Y, θ_y) , where X , Y —horizontal and vertical position in the plane, θ_x , θ_y —horizontal and vertical angle from the beam main axis.

3. BTOR Software and LNB Computational Methods

BTOR (Beam in TORoids) software was developed in 2019 [20] to study neutral beam injection performance in plasma accounting for detailed NB statistics, 3D plasma configuration, and toroidal magnetic field effects. BTOR simulates fast ion population behavior by applying the classical theory of ion deceleration [6], and is capable of delivering, in seconds, any particle ensemble distribution with a detailed resolution. This ‘lite’ approach allows efficient optimization and fine-tuning of beam-plasma operation parameters by applying only straightforward and easily interpreted methods. Despite the natural simplicity of the method, the BTOR results showed good agreement with similar results of ASTRA calculations [22] both for NB ion capture and NBCD efficiency, although the current density in the vicinity of magnetic axis was typically lower when compared to ASTRA profiles [15].

The BTOR package was designed as a set of data flow processing routines, where the particles data passes through transformations, which imitate physical events by applying probability, defined by a relevant cross-section, including atom ionization, fast ion deceleration to thermal velocity, plasma heating, current drive and fusion. This data processing method is referred to as *σ*-approach. With all the probabilities (σ) tabulated or pre-calculated, BTOR methods become deterministic and fast. The statistical model of the neutral beam is referred to as the lite neutral beam (LNB), which will be introduced in more detail through the next sections. In short, the BTOR concept is to study beam-related effects by mixing data processing (*σ*-approach) with efficient analytical or low-order (lite) methods of beam

representation. Here, it should be noted that the scaling laws actively used in the classical tokamak modelling are not always applicable to compact and spherical devices. In plasma physics, ab initio models are assumed to be resource-intensive and time-consuming. However, the reduced numerical ab initio models, such as LNB for beam-driven effects study, can significantly speed up massive calculations while staying within acceptable accuracy.

The LNB beam model takes the beam particles statistics at the plasma entrance (Figure 7), calculated by BTR code, and propagates them step-by-step, i.e., simulates the fast ion (FI) population release and its slowing down. The fast ion distributions in time are converted to energy profiles, which are further used for CD evaluation and neutron source spatial distribution.

Atom ionization in plasma and ion deposition is calculated using the Janev multi-step ionization model [23], with an effective stopping cross-section comprising the main channels of beam ionization on plasma species. The neutral beam intensity attenuation along the beam track is calculated as:

$$\frac{dI}{dx} = -n_e \sigma_s I, \quad (2)$$

where n_e is the plasma target density, and σ_s is the effective beam stopping cross-section due to ionization:

$$\sigma_s = \langle \sigma_{ie} |v - V_b| \rangle / V_b + \frac{n_p}{n_e} (\sigma_{ip} + \sigma_{cx}) + \frac{n_z}{n_e} \sigma_z \approx \langle \sigma_{ie} v \rangle / V_b + \sigma_{ip} + \sigma_{cx} + \frac{n_z}{n_e} \sigma_{iz}. \quad (3)$$

Here, σ_{ie} , σ_{ip} , σ_{iz} are ionization cross sections of atoms in collisions with electrons, protons, and impurities of charge Z, respectively, σ_{cx} is the charge exchange cross section on hydrogen ions, and brackets mean averaging over the Maxwell distribution of electron velocities. Graphs of the beam stopping cross section in the range of FNS-ST plasma parameters are shown in Figure 8. Since the neutral beam energy for FNS-ST is $E_b \sim 100\text{--}140$ keV, the NB is produced from positive ions. After neutralization and dissociation of molecular ions, the beam carries three energy fractions that are shown by violet bars in Figure 8a. It can be seen that for the low-energy fraction $E_{1/3}$, the stopping cross-section can be up to three times higher than that for the full energy fraction (E_{full}), which leads to the ionization and capture of low-energy beam fractions ($E_{1/2}$ and $E_{1/3}$) at the plasma periphery and reduces the total CD output from NBI.

The velocity of fast ions released is decomposed into two components with respect to the magnetic field line: parallel velocity which enables the ion circulation around the torus main axis, and transverse velocity, i.e., orthogonal component associated with the Larmor rotation around the field line. The toroidal current in the plasma is created by the parallel ion velocity. The collisions cause fast ion momentum transfer to plasma electrons and ions. The classical solution for fast ion deceleration due to Coulomb collisions [6] is applied to calculate the fast ions thermalization time (τ_s) as a function of its initial energy E_b , the critical energy E_c , and the value τ_{se} , which is the characteristic Spitzer time:

$$\tau_s = \frac{\tau_{se}}{3} \ln \left[1 + \left(\frac{E_b}{E_c} \right)^{3/2} \right], \quad (4)$$

$$E_c = 14.8 \left(A_b / A_i^{2/3} \right) \cdot T_e, \quad (5)$$

$$\tau_{se} \propto \left(A_b T_e^{3/2} / n_e \right), \quad (6)$$

Here, A_b and A_i are the atom mass of fast ions and plasma ions, respectively, and \propto is means direct proportionality.

E_c is the value of the critical beam energy, which defines the level when the electron and ion heating rates are equal. If the beam ion energy is higher, it loses its energy mainly due to collisions with electrons, with a slight change in momentum, while the scattering

angles of the ions are small. If the ion energy is below the critical level, deceleration occurs mainly due to collisions with plasma ions, and in this case the ion is deflected by significant angles. From Equation (5), the highest value of the critical energy E_c corresponds to the maximum mass ratio of the beam ions to background ions, and directly increases with plasma temperature. For a deuterium beam in a deuterium plasma with $T_e = 5$ keV, the critical energy is ~ 93 keV ($E_c \approx 19 \times T_e$).

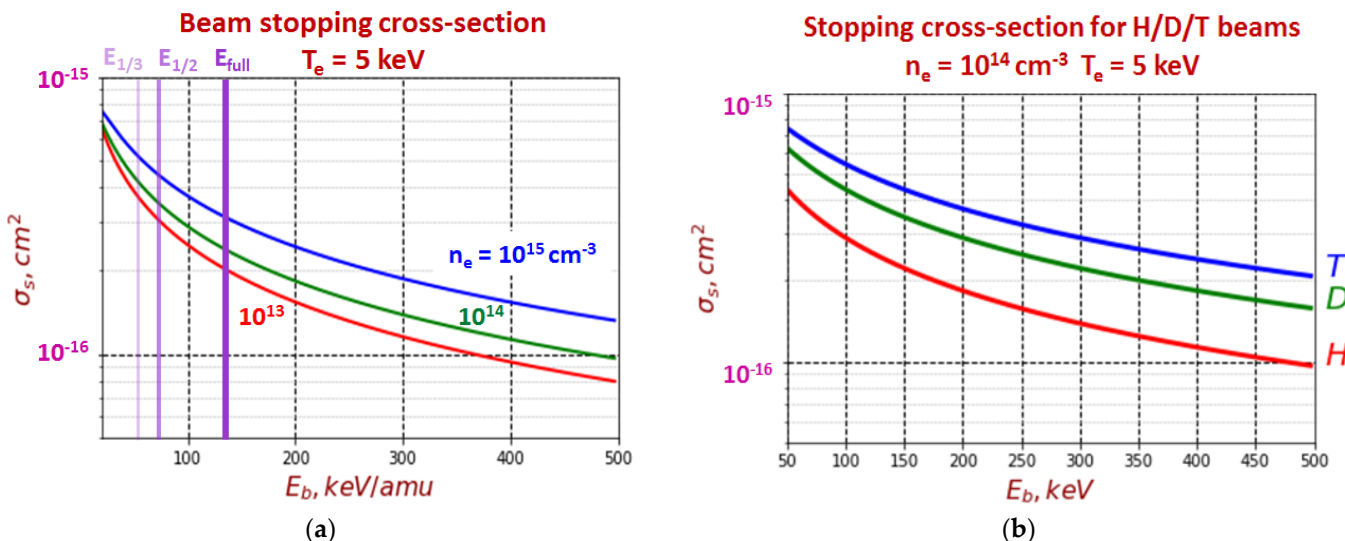


Figure 8. Energy dependence of neutral beam stopping cross section (σ_s , 10^{-16} cm^2) calculated according to the model [23]. (a) Plasma density (n_e) scan, $T_e = 5$ keV, $Z_{\text{eff}} = 1$, with D-beam energy fractions (violet) $E_{\text{full}} = 140$ keV, $E_{1/2} = 70$ keV, $E_{1/3} = 47$ keV; (b) beam specie scan H/D/T, $Z_{\text{eff}} = 1$, $T_e = 5$ keV, $n_e = 10^{14} \text{ cm}^{-3}$.

Fast ion distribution in space and angle can be obtained from a kinetic equation solution with a beam source and a collisional operator, accounting for fast ion deceleration and pitch angle scattering. Instead of the Fokker-Planck solution, LNB calculates the energy distribution (statistics) of fast ions at any 3D point or radial cell, by performing an ion direct ‘deceleration’ in time, and collecting all the partial ion distributions. LNB assumes the background plasma to stay intact and not perturbed by the beam particles. The fast ions are attached to their initial magnetic surfaces, and each follows the magnetic line of their birth.

The geometry of the plasma cross-section in tokamaks is well described by a system of equilibrium magnetic surfaces (MES), as in Figure 9, MES are supposed to be isotherms and isobars. MES contour in the RZ-plane is a function of the reduced minor radius a of the MES and the poloidal angle θ :

$$R = R_0 + \Delta R_{\text{sh}} + a \times \cos(\theta + \delta \times \sin \theta), \quad (7)$$

$$Z = \kappa \times a \times \sin \theta, \quad (8)$$

$$\Delta R_{\text{sh}} = \Delta R_{0\text{sh}} \times (1 - (a/A)^2), \quad (9)$$

Here, κ is MES elongation (ellipticity), δ is triangularity, ΔR_{sh} is the Shafranov shift of axis, i.e., the radial MES axis deviation from the last closed MES axis (LCMS), and R_0 , A , $\Delta R_{0\text{sh}}$ are the major radius, minor radius and Shafranov shift of LCMS. The FNS-ST poloidal plasma cross-section is shown in Figure 9b for $R_0 = 0.5$ m, $\Delta R_{0\text{sh}} = 0.05$ m, $A = 0.3$ m, $\delta_0 = 0.5$, $\kappa_0 = 3$. The MES shapes with negative triangularity ($\delta < 0$), prolate ($\kappa > 1$) or oblate ($\kappa < 1$) MES profiles can be constructed the same way.

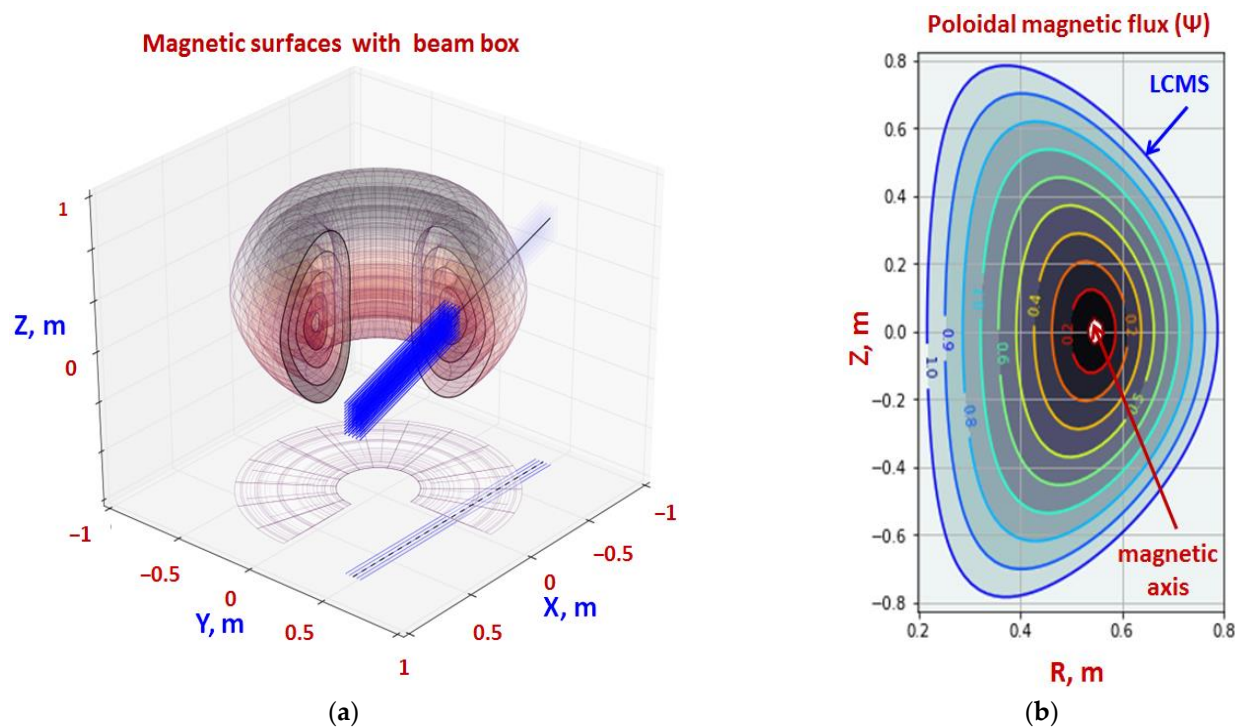


Figure 9. FNS-ST calculation model with plasma magnetic surfaces and the neutral beam box (BTOR). (a) The multi-ray neutral beam model (parallel beam cluster); (b) poloidal plasma cross-section with magnetic surfaces (LCMS is the last closed magnetic surface).

4. Beam Ionization and Fast Ions Deposition

The model of NB multi-step ionization described in the previous section was applied to the calculation of fast ion release rates within the injection channel, which is the plasma volume containing the NB atom tracks. Beam atoms that pass the plasma without ionization create shine-through power losses. They produce a thermal load on the first wall of the tokamak chamber, which has to be evaluated for all possible scenarios of tokamak operation, especially in transient regimes with low plasma density.

In a low aspect ratio tokamak, the beam spatial geometry and the internal angular structure (beam shaping), when combined with magnetic field topology effects, result in a complex beam deposition footprint, with a 3D structure completely different to “thin” beam geometry (or single ray beam). Therefore, the profiles of beam-driven current and neutron generation in compact and spherical devices cannot be approximated by thin (pencil-type, or narrow) beams, which can be a reasonable reduction for higher aspect devices, such as ITER. The beam finite size impact is illustrated in Figures 10 and 11, in which the beam attenuation, the fast ion release rate, and the resulting current are shown for thin (single ray) and thick ($0.3 \times 0.6 \text{ m}^2$) beam options. Figures 10a and 11a show the profiles along the NB axis, while Figures 10b and 11b show the corresponding radial profiles in plasma poloidal cross-section (RZ-plane).

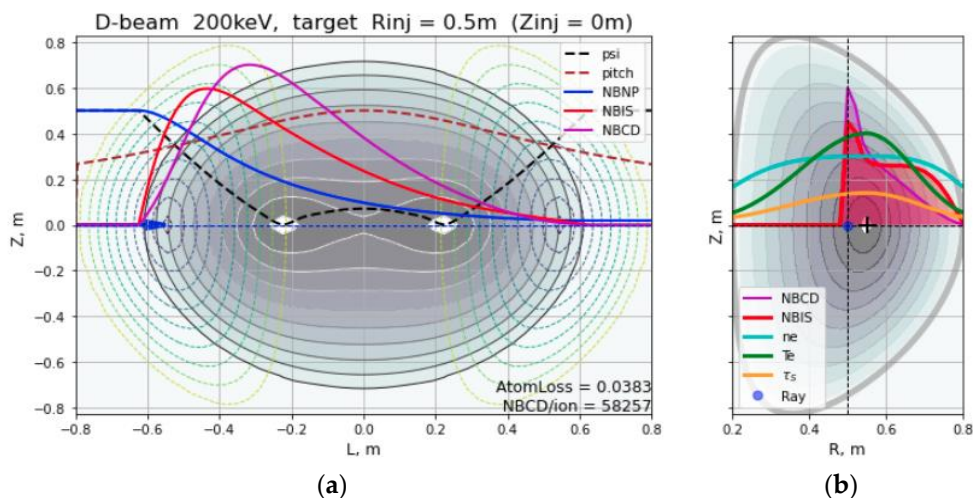


Figure 10. Profiles of thin beam (single ray) penetration (BTOR): (a) along the horizontal axis; (b) the correspondent radial profiles in a poloidal cross-section.

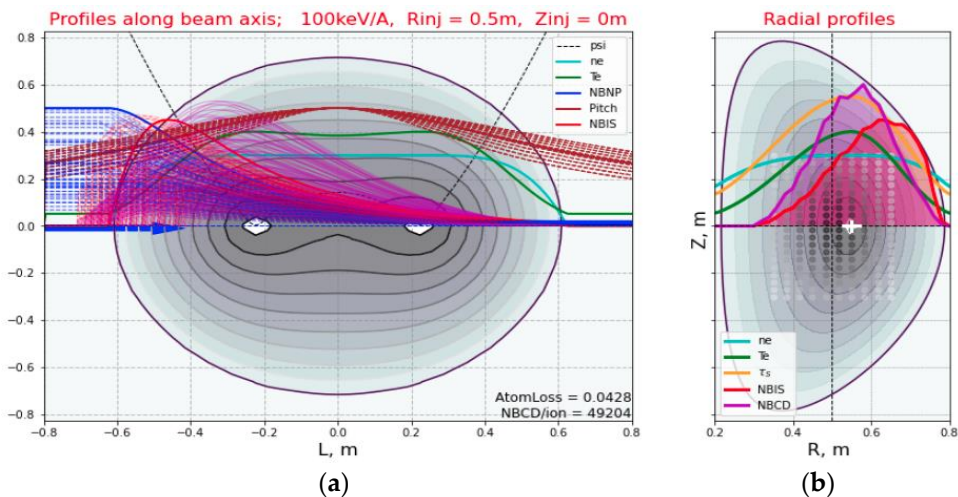


Figure 11. Profiles of thick beam (real shape) penetration (BTOR): (a) along the horizontal axis; (b) the correspondent radial profiles in a poloidal cross-section.

The beam ionization footprints (2D) in poloidal RZ-plane for thin and thick beam options are shown in Figure 12 for deuterium beam energy $E_b = 200$ keV, and for the beams on-axis targeting. It can be seen that these two beam options produce not only different shapes of the injection channel, but also different radial profiles of beam ionization (shown in red).

Figures 10 and 11 also illustrate the change of the ion initial pitch cosine, i.e., the angle cosine between the initial ion velocity and the local magnetic field vector. This value is also impacts NBCD calculation, since it defines a parallel velocity component driving the current. With a finite beam thickness and internal angular dispersion (NB shaping effects), the ionization rate and total amount are varied across the tangential chords within the injection channel, due to difference in time of flight, plasma density along the chord, and pitch angle scatter. The beam shaping effects are also responsible for thermal load high asymmetry and power peaking at the tokamak first wall, which is produced by a non-uniform distribution of shine-through beam power losses along different NB rays tangential chords.

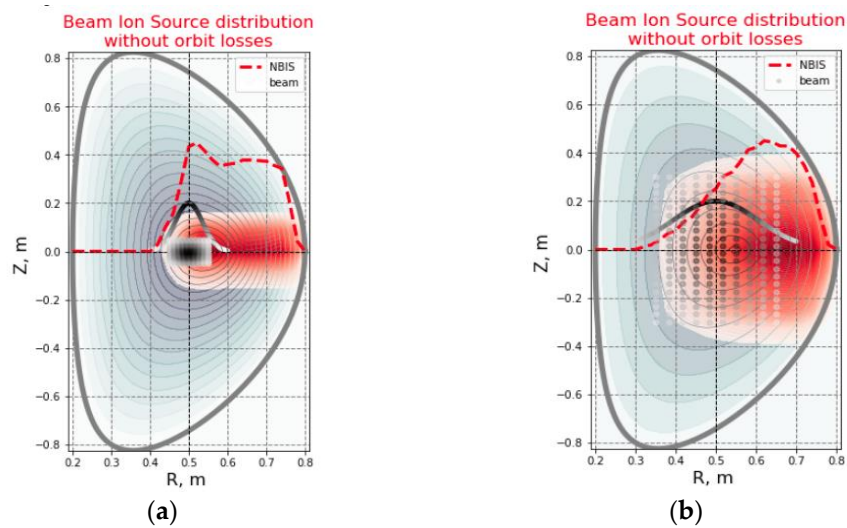


Figure 12. Neutral beam ionization in plasma poloidal cross-section for deuterium beam, $E_b = 100 \text{ keV/amu}$ (BTOR): (a) thin beam $10 \times 10 \text{ cm}^2$, (b) thick beam $30 \times 60 \text{ cm}^2$.

5. Neutral Beam Shine-Through Power

Shine-through beam losses and the associated thermal load onto the first wall serve as severe restrictions for the injected beam energy choice for efficient current drive and enhancing nuclear fusion in any tokamak. Figure 10 is an illustration that fast ion deposition within the plasma inner core, which is most favorable for current drive, is a result of a sufficient atom penetration depth into plasma. On the other hand, the beam deep dive to plasma core also means a higher fraction of non-ionized atoms, and thus raises the risk for the tokamak chamber first wall to be burnt by the residual neutral power.

For the FNS-ST tokamak, a quite moderate range of beam energies of 100–150 keV is not the best for current drive and neutron generation, but this energy level ensures safer tokamak operation compared to a more efficient beam energy range above 200 keV. Maximum NBCD efficiency in tokamak is achieved normally in the diapason of energy ratio $E_b/E_c = 2–5$ [5], which implies the optimal beam energy for $T_e = 5 \text{ keV}$ should be 200–500 keV, which would be not acceptable in terms of the direct power densities faced by the first wall.

The beam ionization deposition in FNS-ST plasma (thick beam $30 \times 60 \text{ cm}^2$, $E_b = 120 \text{ keV}$, $n_e = 10^{20} \text{ m}^{-3}$) is shown in Figure 13 mapped onto the horizontal (a) and vertical (b) planes containing the beam axis. The horizontal footprint proves the ionization rate to be strongly non-uniform over the beam cross section, with less total ions released along the rays coming closer to outer plasma edge. This effect raises the residual neutral power and enhances the power load asymmetry on the first wall, which is already biased due to the wall inclination with respect to the beam axis.

The resulting power load profiles on the FNS-ST first wall are shown in Figure 14 for two operation cases: with ideal beam alignment and with a beam nominal misalignment of $4/-6 \text{ mrad}$ (the error deviation from the ideal beam focusing in horizontal and vertical planes due to technology reasons). From Figure 14b, one can expect the beam alignment errors to lead not only to the direct power losses and higher loads within the injector beamline, but also to affect the shine-through power profile, and, in some cases, they can increase the peak power density onto the first wall by ~ 1.5 times (see the figure caption).

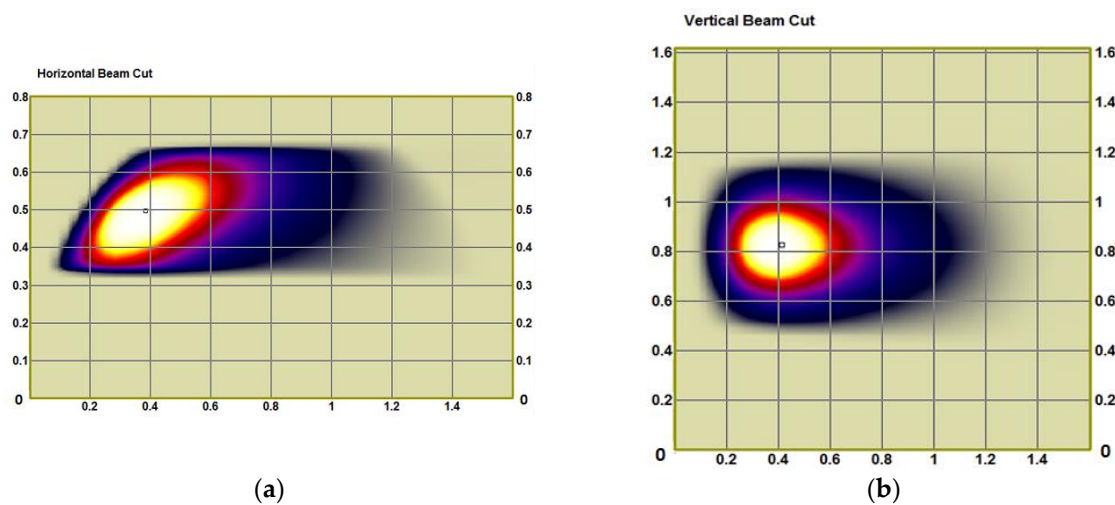


Figure 13. Neutral beam spatial deposition in FNS-ST plasma in the planes containing the beam axis (BTR plots): (a) horizontal plane, (b) vertical plane. The horizontal axis on both images indicates the length along the beam axis (meters) from the NB port. The vertical axis indicates the horizontal distance from tokamak center (a), and the relative height (b) from the level $Z = -0.8$ m.

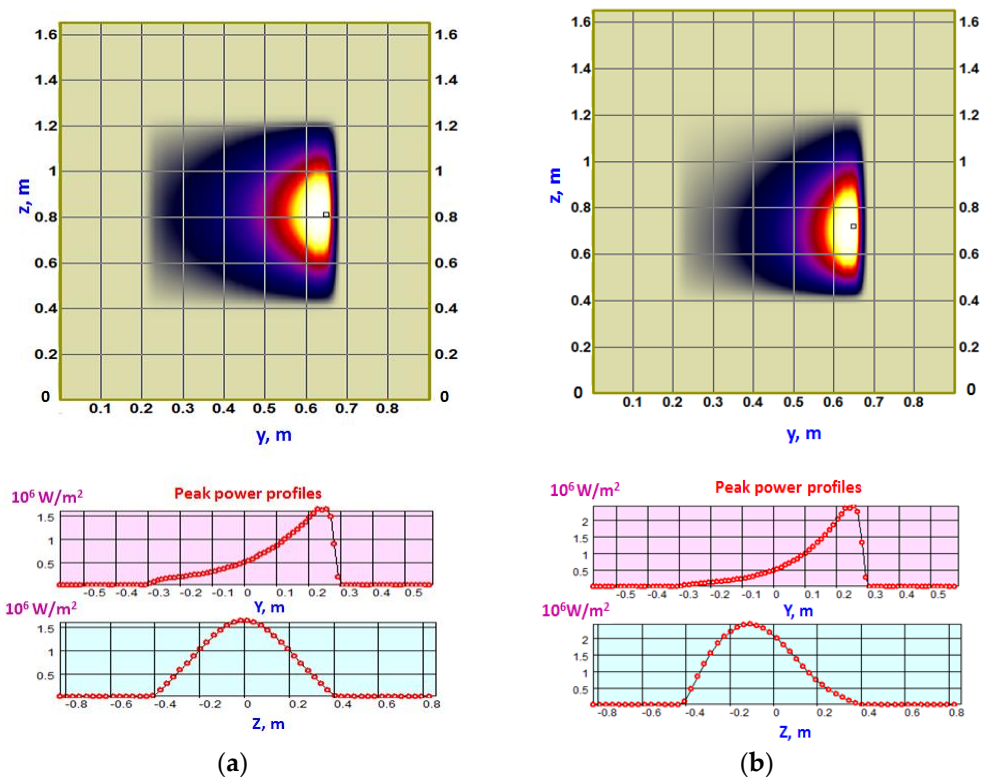


Figure 14. NB shine-through power density maps at FNS-ST first wall (NB port size $0.3 \times 0.6 \text{ m}^2$) in two operation cases: (a) ideal beam alignment, total power— 0.147 MW , peak density— 1.65 MW/m^2 ; (b) t beam nominal misalignment (error) $4/-6$ mrad in horizontal and vertical planes, total power— 0.167 MW , peak density— 2.43 MW/m^2 . For BTR power density profiles, the axes X, Y and Z correspond to NBI coordinates shown in Figure 2.

Shine-through neutral power was also evaluated for the reduced injection port size $0.2 \times 0.4 \text{ m}^2$. With the expected decrease of the power injected, the shine-through power dropped by a factor of two, and the peak power density on the first wall falls by ~ 1.5 times (see the caption to Figure 15).

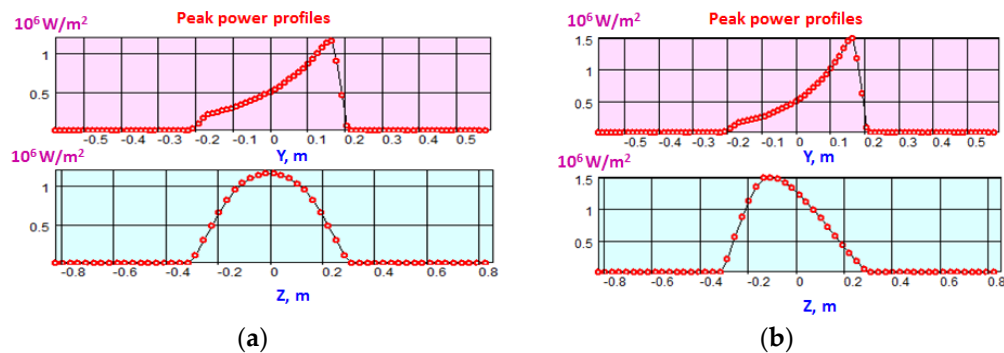


Figure 15. NB shine-through power density maps at FNS-ST first wall (NB port size $0.2 \times 0.4 \text{ m}^2$) in two operation cases: (a) ideal beam alignment, total power—0.070 MW, peak density— 1.16 MW/m^2 ; (b) beam nominal misalignment (error) $4/-6 \text{ mrad}$ in horizontal and vertical planes, total power—0.069 MW, peak density— 1.50 MW/m^2 . For BTR power density profiles, the axes X, Y and Z correspond to NBI coordinates shown in Figure 2.

Finally, the shine-through power density profile sensibility to the beamlet horizontal focusing was evaluated. For this, all beamlets were aimed parallel in the horizontal plane (Figure 16). The injected beam power to plasma decreased by only -5% , with a correspondent reduction in peak shine-through power density. However, the effect was not pronounced, so additional study is needed.

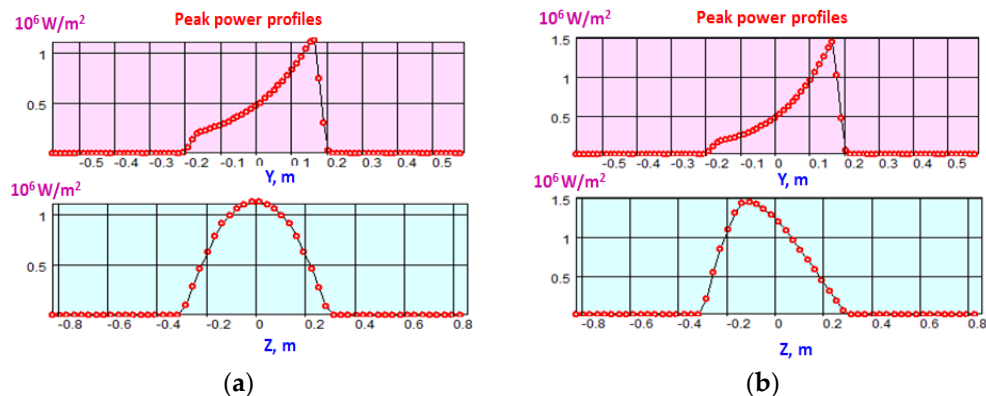


Figure 16. NB shine-through power density maps at FNS-ST first wall for parallel beamlet aiming (NB port size $0.2 \times 0.4 \text{ m}^2$) in two operation cases: (a) ideal beam alignment, total power—0.066 MW, peak density— 1.13 MW/m^2 ; (b) beam nominal misalignment (error) $4/-6 \text{ mrad}$ in horizontal and vertical planes, total power—0.065 MW, peak density— 1.45 MW/m^2 . For BTR power density profiles, the axes X, Y and Z correspond to NBI coordinates shown in Figure 2.

The beam energy and plasma target density range were restricted not only by the risk of chamber first wall damage, but also by the physical parameters of equilibrium and stability. Within the frame of this work, the steady-state and stable operation of the plasma-beam system were assumed to be maintained, and stability analysis was not performed.

6. Fast Ions Losses and Toroidal Effects

In the FNS-ST compact tokamak design, plasma is confined by a toroidal magnetic field of about 1–1.5 T. Moderate field values impair the fast particles confinement, especially at the plasma low field side. In spherical tokamaks, in contrast to the conventional (i.e., higher aspect ratio) tokamaks, the toroidal magnetic configuration causes the essential fraction of ions captured towards the trapped orbits, which are not closed around the MES axis. The trapped (or unclosed, or banana) particle fractions, as opposed to the population of passing particles, drive no direct current in the toroidal direction. The orbital losses of

fast particles in spherical tokamaks typically exceed those in conventional tokamaks by several times.

The initial fast ions energy released in FNS-ST from NB atom injection is $\sim 100\text{--}150$ keV. Their Larmor radius in a magnetic field of ~ 1 T is about several centimeters, so the fast ions born at the plasma periphery with a small pitch angle cosine escape from being captured by plasma already during the first Larmor circle. When the number of rescued ions is large, the total efficiency of NB heating and current drive decrease according to the lost ion fraction. The minimum (or critical) pitch angle cosine value, allowing the ion to be captured within the separatrix, i.e., the last closed magnetic surface (LCMS), is evaluated for a given beam particles energy and the magnetic field configuration. Based on the critical pitch, the lost ions fraction due to Larmor rotation is calculated for a given injection geometry defined by the beam shape and tangential aiming. A similar procedure is applied to the calculation of bounding pitch for ions passing, and to the trapped (banana) losses estimation. The beam fast ions with a pitch cosine less than the critical value are considered to be lost (or cut-off) within the “loss cones”. Note the loss cone in a toroidal magnetic trap is inverted compared to the loss cone in mirror plasma devices. The fast beam ions trapped to banana trajectories, together with the ions escaping on the first Larmor, are considered as not driving the toroidal current, but they are supposed to contribute to the neutron generation.

Accurate fast ion drift simulation is very expensive, especially in spherical tokamaks where the fast ion Larmor radius is comparable to the magnetic field inhomogeneity scale, and the drift approximation is not very applicable. BTOR implements the following simple procedure which boosts the fast ion loss evaluation speed: the fast ion loss diagram for a given magnetic configuration is calculated (Figure 17a), the two-dimensional distribution of the ion source over the radial coordinate (ψ) and pitch angle cosine (Figure 17b,c) are reconstructed, and finally both maps are overlapped (yellow shade in Figure 17c).

The fast ion tracks are reconstructed by BTOR by combining the circulation along the field line and Larmor rotation. The example ion orbits in the FNS-ST tokamak configuration for a reduced magnetic field value ($B = 0.5$ T, to make the Larmor radius wider) are shown in Figure 18a,b; they correspond to the ion passing along the magnetic line without collisions. Figure 18a refers to the fast ion released at the periphery, while Figure 18b shows the orbit of fast ion born in the vicinity of the magnetic axis. In the first case (Figure 18a) the ion is produced with a lower pitch cosine and, if it does not escape from the plasma at the first Larmor, it can be captured either to passing or to a trapped orbit depending on the poloidal coordinate of the birth. The fast ion released closer to the magnetic axis (Figure 18b) is passing, as its velocity vector is more parallel to the magnetic field vector and almost equal to the maximum pitch cosine value (see Figure 18c), while the mirror ratio at the axis is minimum: $\Pi = B_{\max}/B_{\min} \sim 1$.

The overall number of fast ions lost in spherical tokamaks due to orbital effects can reach 70–80%. These losses strongly depend on the beam energy, the NB shape and aiming geometry (radius, axis inclination). While Larmor losses can be reduced by increasing the magnetic field, ion capture onto trapped orbits is predetermined by the toroidal magnetic configuration and, therefore, cannot be totally avoided. For given tokamak parameters, the beam energy and aiming can be tuned to reduce overall beam losses and increase NBI performance. It should be noted that the optimum conditions for NBCD and for neutron generation typically differ and even necessarily overlap in parameter space.

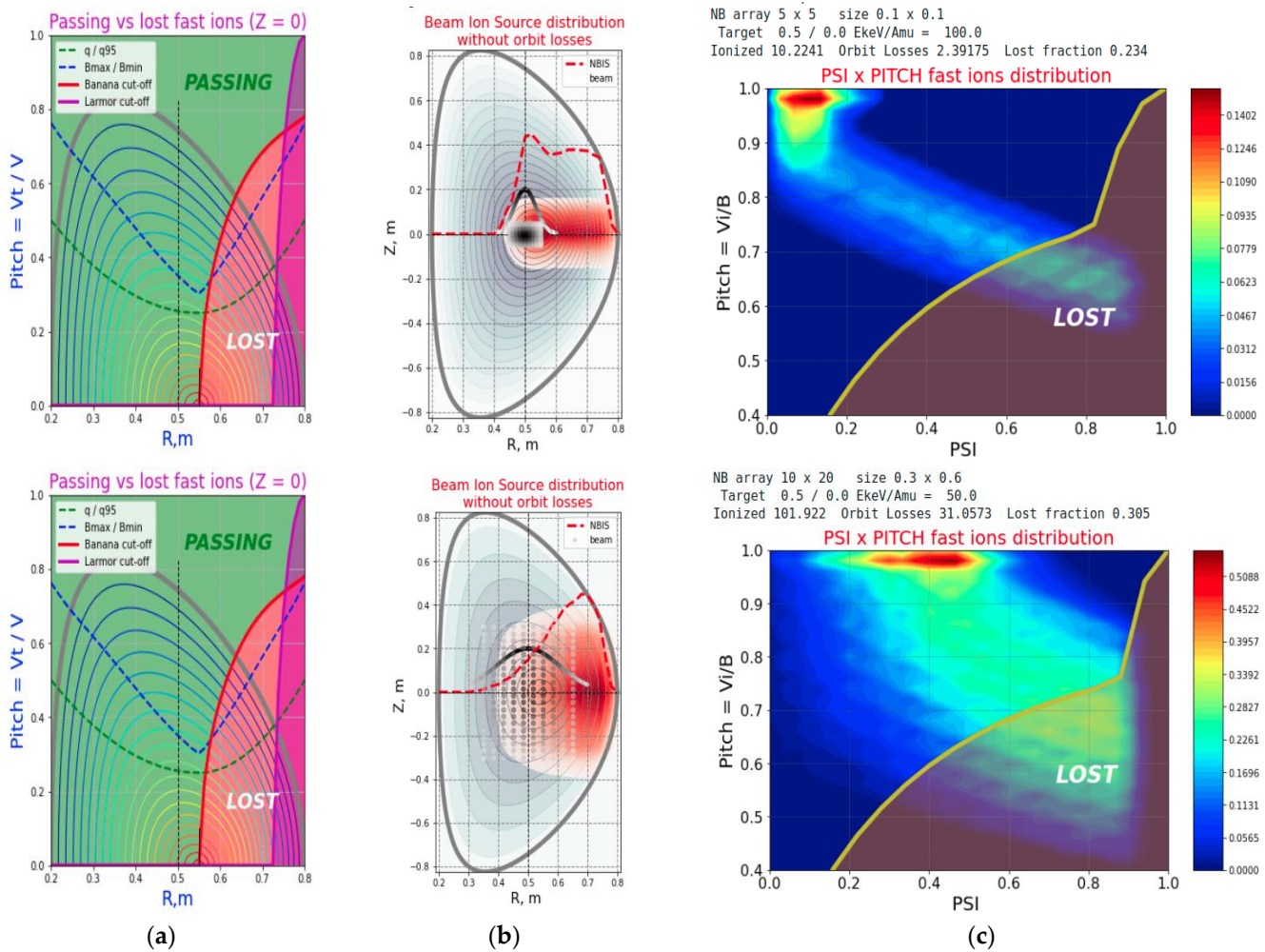


Figure 17. Fast ion orbital loss computation in BTOR: (a) loss cones due to Larmor (red) and banana (purple); (b) ion source distribution in a poloidal plane; (c) ion source over the radial coordinate (ψ) and pitch angle with overlapped loss cones (yellow shaded). Upper row = thin beam; lower row = thick beam $30 \times 60 \text{ cm}^2$.

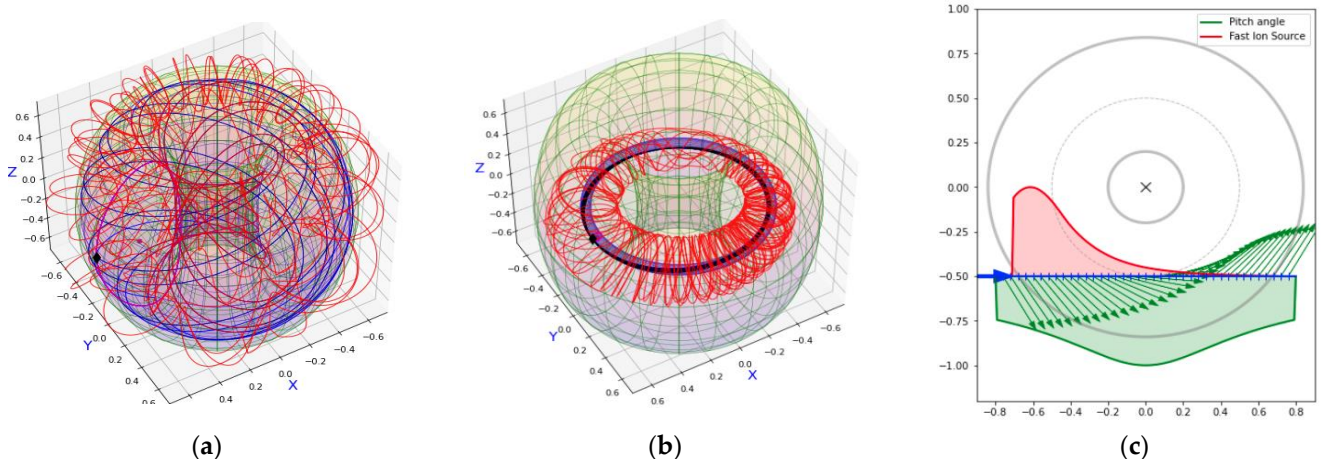


Figure 18. Fast ions orbits (BTOR plots): (a) at the plasma periphery (low magnetic field B_t , low pitch cosine); (b) at the plasma core (high B_t , high pitch cosine). (c) The magnetic vector direction (green arrows), beam ray pitch cosine variation (green profile) along the beam ray (blue arrow), and the fast ion release profile along the beam ray (red).

For fast ions slowing down in plasma, neoclassical (toroidal) effects occur by magnetic field variation along the magnetic field line. For low inverse aspect ratio ($\varepsilon = r/R$) values, in the area close to the magnetic axis the toroidal effects almost vanish, while they grow at the plasma periphery. The ion current toroidal correction produces an additional strong impact on the current drive profile and the overall beam efficiency [24]. For each MES with a specific ε -value, the fast ions with a pitch cosine below the critical level (see Figure 17a) are trapped to banana orbits and do not drive toroidal current. Fast ions with a higher pitch cosine go on passing and circulating around the main toroidal axis. Their parallel velocity oscillates cyclically during their motion along the magnetic field line (see Figure 19), and the amplitude of oscillation depends on the pitch cosine at B_{\min} point (at the poloidal coordinate $\Theta = 0$) and on the magnetic field mirror ratio $\Pi = B_{\max}/B_{\min}$ along the magnetic field line.

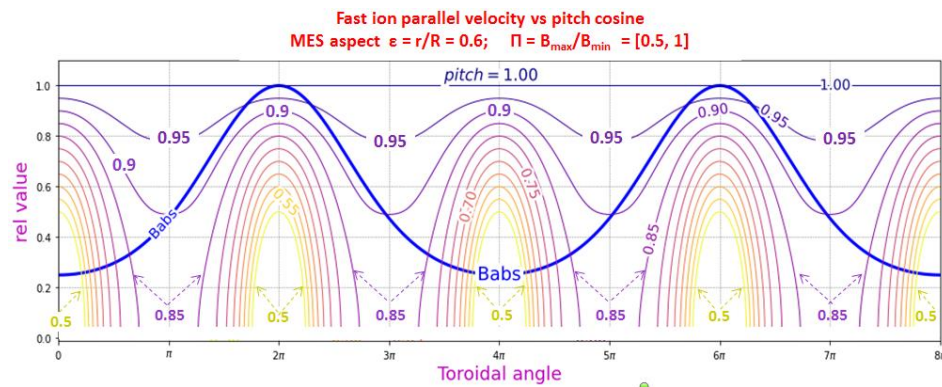


Figure 19. Fast ion parallel velocity variation along the magnetic line on a magnetic surface with $q = 2$, $\varepsilon = r/R = 0.6$, for different pitch cosine values in the interval $[0.5, 1]$.

Figure 19 shows that the decrease of the average parallel velocity of the fast ions circulating around the torus, even without accounting for deceleration, depends on the ion initial pitch angle and on the MES mirror ratio $\Pi = B_{\max}/B_{\min}$. The effect of field line twisting angle was also studied, but its influence on NBCD proved to be not as pronounced compared to the mirror ratio impact, as shown in Figure 20.

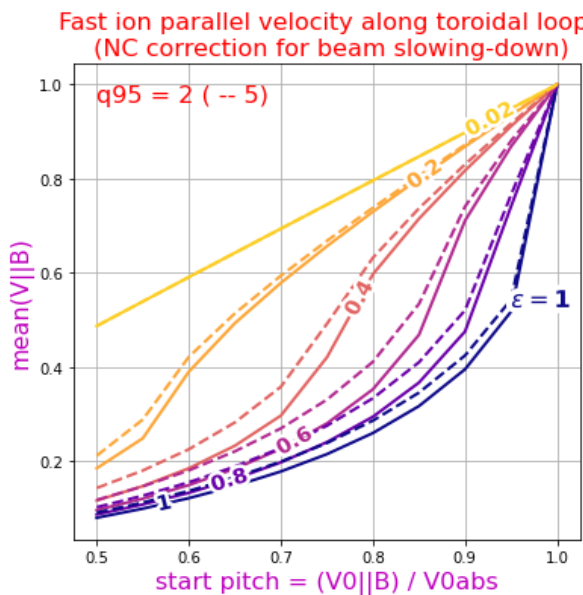


Figure 20. The fast ion parallel velocity decline due to toroidal field geometry: inverse aspect ratio scan ($\varepsilon = r/R$) for $q_{95} = 2$ (solid), $q_{95} = 5$ (dashed).

For total NB current drive estimation, the electron current drive in the opposite direction should be also taken into account. Due to the same toroidal effects, which reduce the direct ion current, the electron current is reduced as well. While neoclassical ion current decreases with increasing ϵ , the electron current compensation also drops with ϵ increase. While classical theory predicts zero current for a hydrogen beam injected to a pure hydrogen plasma ($1 - Z_b/Z_{\text{eff}} = 0$), the neoclassical approach states non-zero NB current even for pure hydrogen plasma ($Z_{\text{eff}} = 1$). However, within the frame of this work, the electron current correction was not evaluated.

7. Fast Ion Distributions in Energy

Since nuclear fusion between fast beam ions and thermal plasma ions is the main source of neutrons in FNS-ST tokamak, the fast ions energy distribution function (EDF) should contain an essential population with higher energies, or “hot tail” fraction, with a longer thermalization path and more probability to fuse until thermalization. The hot tail fraction grows when the beam is predominantly ionized and captured to passing orbits, and maximum neutron yield is achieved when all the beam rays are captured to passing tracks. The main steering parameters here are the beam energy and plasma density, with the operation range limited by the physical scenario and engineering aspects, such as the first wall overheating risks.

Figure 21 shows the EDF of a deuterium beam for different energy ratios between the beam and plasma ions E_b/T_e (for a fixed plasma density $n_e = 1 \times 10^{20} \text{ m}^{-3}$). Thin colored lines correspond to the partial contribution of individual groups of slowing ions depending on the radial coordinate of their birth and circulation, whereas the bold black line shows the integral energy distribution across the slowing ions ensemble. Along each beam ray (atom track), the ion energy profile shape depends on the ion release radius (see Figure 21). A distribution peak at low energies can be normally observed for cold peripheral plasma layers, and a monotonic increase is more typical for the hotter core plasma layers. The larger the ratio (E_b/T_e) the smaller is the relative fraction of fast particles in the integral distribution, as is clearly seen from Figure 21b. The plasma temperature decrease for a fixed beam energy E_b leads to an expansion of a relatively cold plasma region from the periphery ($\Psi = 1$), which results in the hot tail decay in EDF.

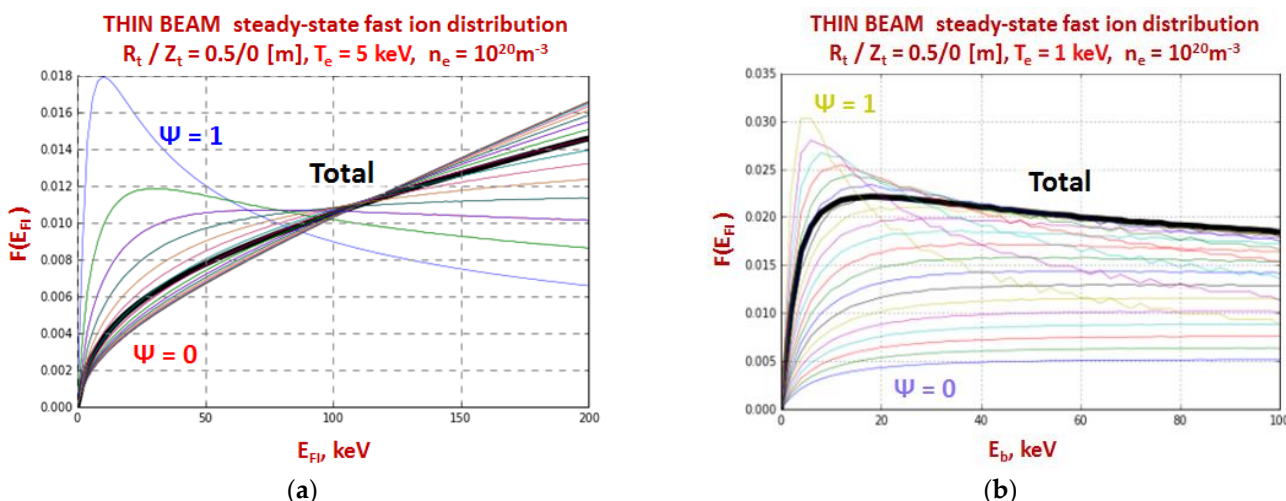


Figure 21. Fast ion energy distribution function from the beam injected tangentially along the major tor radius in FNS-ST ($R_t = 0.5 \text{ m}, Z_t = 0$) with plasma density $n_e = 1 \times 10^{20} \text{ m}^{-3}$ for different plasma temperatures: (a) $T_e = 5 \text{ keV}$, (b) 1 keV .

8. Neutral Beam Current Drive and Neutron Generation in FNS-ST

With the beam finite spatial width and the internal angular spread, the fast ion population distribution in phase space is rather complex and cannot be simply extrapolated

from a thin beam option, especially for low aspect ratio systems. The initial distribution of fast ions and their velocity change along circulation, affected by the low aspect toroidal field, result in specific NBCD and neutron generation profiles, which are not specific for the conventional tokamak design. The total current drive and neutron yield in these systems are more sensitive to the beam shape. The beam thickness impact on NBCD in FNS-ST is illustrated in Figures 10–12 for $E_b = 100$ keV/n.

The FI path length in plasma and the driven current are roughly proportional to the ion slowing down time (τ_s). Thus, the optimal conditions for current drive are naturally achieved for high beam relative energy ($E_b/T_e \gg 1$), high plasma temperature and low plasma density, while the plasma density lower limit should be correlated with the beam energy (see Section 5). Figure 22 shows the influence of NB energy on the radial profile of the beam ion deceleration time, beam atom ionization and current drive. The overall current amplification due to FI circulation depends on the NB energy and on τ_s profile.

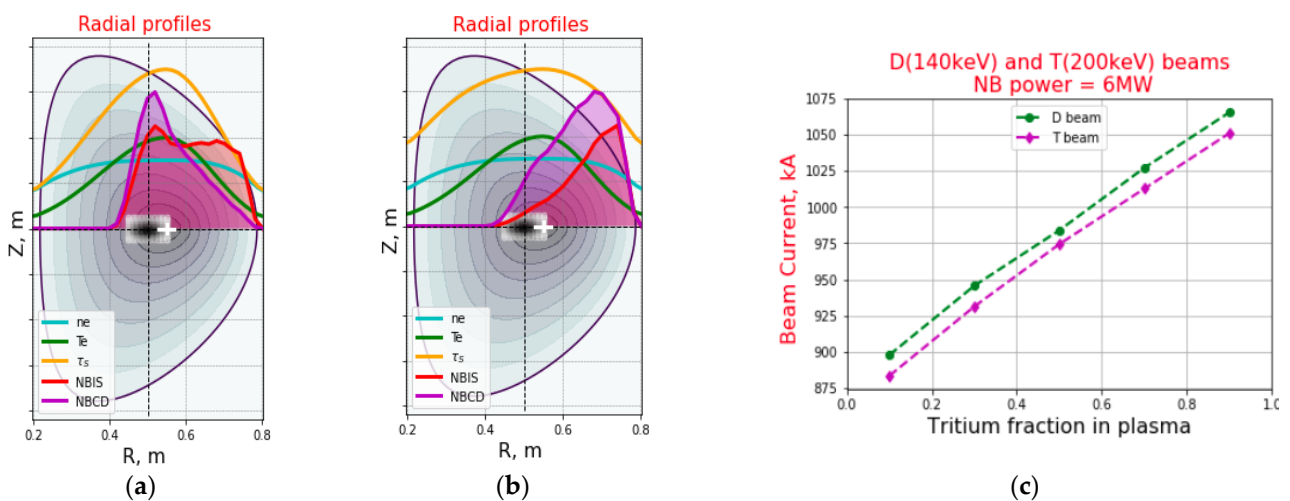


Figure 22. Radial plasma profiles (temperature T_e , density n_e), fast ion deceleration time (τ_s), ion source intensity, and fast ion current in FNS-ST driven by a thin deuterium beam with different energy E_b : (a) 200 keV; (b) 50 keV; (c) deuterium ($E_b = 140$ keV) and tritium ($E_b = 200$ keV) beam driven current against tritium fraction in DT plasma, for the NBI power $P_b = 6$ MW.

The initial fast ion orbital losses (see Section 6), including FI escape from the first Larmor circle and trapping to banana trajectories, reduce the current drive. The associated losses can be estimated with the fast ion release distribution map (Figure 17c). For spherical systems these losses amount to 70–80% if the NB energy is relatively low. The toroidal effects additionally reduce FI parallel velocity responsible for NBCD down by 20–30% (see Figure 20).

If the atomic beam is produced from positive source ions (see Section 2), normally it consists of three energy fractions (E_{full} , $E_{1/2}$, and $E_{1/3}$), contributing to the integral profiles of beam ionization, NBCD, and beam-plasma fusion. The NBCD efficiency of the three-component neutral beam was studied in detail in [25], with the NBCD estimated in FNS-ST plasma for the beam energy range $E_b = 100$ – 140 keV accounting for NB composition. Figure 22c illustrates the NBCD scans against tritium fraction in DT plasma target.

In the FNS-ST neutron source design, up to 99% of the primary neutrons are expected to come from fusion between the fast beam ions and thermal background plasma, while thermal (cold) plasma is evaluated to produce ~1% of total fusion rate; the thermal share in neutron yield can be boosted by rising the plasma temperature. The fast ion distribution in energy space (Figure 21) allows one to obtain the relative fast ion velocity distribution in plasma, and to calculate the beam-plasma fusion rates. The neutron source operation scenario presumes that the fast ion slowing down time exceeds the plasma energy confinement time; thus, the probability of a fusion act involving a fast ion (which can be called

FI “reactivity”) exceeds the probability of fusion between thermal plasma ions by factor of 10–100.

The neutron emission rate in beam-plasma fusion depends on the hot tail contribution to the EDF, the ion deceleration time, and the target ion density (tritium target for deuterium beam, and deuterium target for tritium beam). Typically, the operation windows for optimum NBCD, and for the beam-plasma fusion, correspond to different parameter ranges, and multi-parametric optimization is needed to find the parameters intervals possible overlaps.

The neutron source distribution from a deuterium beam envelope $0.1 \times 0.3 \text{ m}^2$ ($E_b = 200 \text{ keV}$) is shown in Figure 23, for different cases of NB steering into FNS-ST. When the beam axis is targeted to the tangential point with a radius less than the plasma major radius (a), the neutron source distribution is most uniform over the plasma core, while outward beam targeting (c) results in neutron emission concentrated in a radial layer. For a beam directed on-axis (b) the neutron source has a peak in the vicinity of magnetic axis.

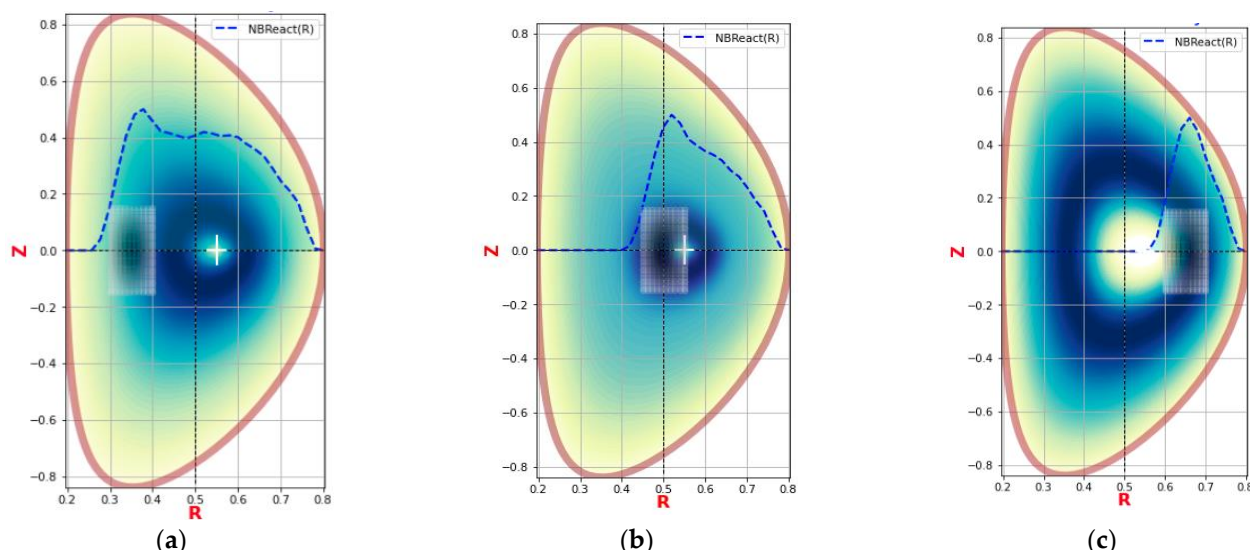


Figure 23. Neutron source distribution from a deuterium beam $0.1 \times 0.3 \text{ m}^2$ ($E_b = 200 \text{ keV}$) for different beam tangential aiming: (a) $R_t = R_0 - 0.5a$; (b) $R_t = R_0$; (c) $R_t = R_0 + 0.5a$.

For a neutral beam produced from positive ions and composed of three energy components (E_{full} , $E_{1/2}$, and $E_{1/3}$), the specific contribution of each beam fraction to neutron yield was evaluated. The beam spatial thickness and the energy composition impact on the neutron output in FNS-ST plasma is shown in Figure 24. The atomic beam with cross-section $0.3 \times 0.6 \text{ m}^2$ and composed of three fractions produced half the neutron yield compared to the thin mono-energetic beam option (at $E_b = E_{\text{full}}$).

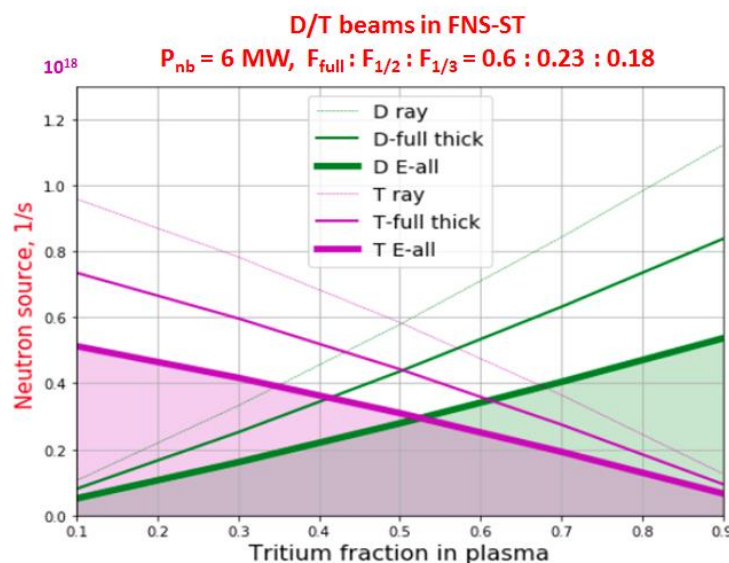


Figure 24. The impact of neutral beam spatial thickness and energy composition on the neutron output in FNS-ST as a function of tritium fraction in DT plasma: deuterium beam ($E_b = 140 \text{ keV}$) is shown green, tritium beam ($E_b = 200 \text{ keV}$) is shown purple. The beam energy fractions are $F_{full}/F_{1/2}/F_{1/3} = 0.6/0.23/0.18$.

9. Optimum NB Injection Parameters for FNS-ST Tokamak

The NB parameters can be optimized for the following target criteria: the NB production efficiency in the injector unit, the injected power density, the beam current drive efficiency in plasma, the overall current drive value and profile, the beam reactivity, the beam-plasma fusion rate, or the total neutron yield. Neutral beam injection can be also optimized for plasma current profile control, as it can directly generate a localized off-axis current.

For a thin beam model, when the beam cross-section is small compared to the plasma cross-section, the best NBCD efficiency is expected when the fast ion population release and circulation are concentrated in the area where the beam axis is tangential to the magnetic field lines, i.e., the pitch cosine value is maximal. In this case the optimization is simply reduced to adjusting the values of beam energy, axis aiming, and the plasma density along the beam path. However, for a real shape (or thick) beam model, the optimization approach is quite different. This includes the parametric study of the beam driven response in plasma, which is gathered from a great number of beam rays (up to 10^9); the procedure is repeated for each parameter scanned. The toroidal field topology and the beam shape effects play the major role in beam-driven response, as was described in the previous sections. Our analysis has shown that a deuterium beam with an energy of $\sim 150 \text{ keV}$ and higher would be more efficient for NBCD and neutron emission in an FNS-ST tokamak, since it creates a fast ion population located closer to the plasma axis, where the ion deceleration path is maximum; however, the NB production technology has low efficiency at the energy range $150\text{--}200 \text{ keV}$ for the preferable beamline design based on a positive ion source [21].

The results of NB response analysis are shown in Table 2, where the beam energy and beam aiming radius are used as parameters to scan. The efficiency of axial injection (i.e., aimed tangentially to the major plasma radius, $R_t = R_0$) of a deuterium beam injected at the energy $E_b = 150 \text{ keV}$, is the best both for NBCD and neutron emission. For lower beam energy (or higher plasma density), the beam is mainly captured at the plasma periphery. In this operation mode, the initial orbital losses of fast ions reduce the NBCD essentially (by $\sim 75\%$ at $E_b = 25 \text{ keV}$), and therefore it is more efficient to steer the beam outwards from the plasma axis (to the low field side), because the beam initial losses are reduced due to increasing the initial pitch cosine of the FI population. However, for higher neutron emission, the FI deposition should be shifted inside from the plasma axis (as is clear from Figure 23a), where the internal plasma layers with more dense plasma boost the fast ion

reactivity. We can conclude that the maximum neutron yield from the beam-plasma fusion can be expected for NB intra-axial aiming, although the NB current drive can be reduced down by three times compared to the optimum value.

Table 2. Fast deuterium beam losses and performance in FNS-ST plasma $B_0 = 1.5$ T, $T_e = 5$ keV, $n_e = 10^{20}$ m⁻³, beam cross-section 0.1×0.3 m².

| Aiming Radius, m | Shine-Through Losses, % | Fast Ions Orbital Losses, % | Current Drive per $P_{inj} = 1$ MW, kA | Neutron Yield per $P_{inj} = 1$ MW, n/s |
|---|-------------------------|-----------------------------|--|---|
| Beam Energy $E_b = 150$ keV | | | | |
| 0.35 | 1.6 | 42 | 134 | 1.06×10^{17} |
| 0.5 | 2.8 | 29 | 170 | 1.07×10^{17} |
| 0.65 | 9.4 | 12 | 151 | 8.3×10^{16} |
| Beam energy $E_b = 100$ keV | | | | |
| 0.35 | 0.32 | 51 | 88 | 5.75×10^{16} |
| 0.5 | 0.7 | 36 | 126 | 5.71×10^{16} |
| 0.65 | 3.9 | 14 | 140 | 4.66×10^{16} |
| Beam energy $E_b = 50$ keV | | | | |
| 0.35 | 10-4 | 73 | 28 | 7.1×10^{15} |
| 0.5 | 0.01 | 56 | 50 | 6.9×10^{15} |
| 0.65 | 0.3 | 20 | 96 | 6.2×10^{15} |

10. Conclusions and Outlook

To study the geometry impact on NB response and performance in tokamak plasmas, we propose a light-weighted technique of multi-ray beam tracing (LNB), which strikes a balance between the best features of the advanced NBI models, including high accuracy, flexibility, almost real-time performance, and the ability to be integrated into a calculation workflow. The LNB is implemented in BTR-BTOR software dedicated to NBI design and beam-plasma interaction in tokamaks.

The approach was applied to study the beam-plasma effects in a compact neutron source based on an FNS-ST spherical tokamak with a special focus on the toroidal field and the neutral beam shaping issues. The LNB model of NB injection comprised detailed beam statistics (up to 10^9 particles) and evaluated the beam losses and performance in plasma by implementing straightforward and efficient methods of massive data processing.

LNB analysis of FNS-ST tokamak clearly revealed that fast ion distribution in plasma and the overall NBI performance should be sensitive to beam-plasma geometrical aspects, including the plasma core toroidal aspect ratio, beam envelope geometry, beam angular divergence and axis aiming. While our approach is applicable to NBI optimization and coupling in conventional tokamak systems, shaping issues have proved to be more pronounced and essential for low aspect tokamak design, and in particular for smaller spherical systems such as FNS-ST. For a compact tokamak design, the NB optimization procedure is generally more complex due to the energy composition of the injected beam, which results in beam-plasma interaction splitting into several channels according to the beam composition. Each beam fraction produces its own fast ion population in plasma, and these populations interact in a different manner with the toroidal magnetic field and with plasma background.

The optimal interval of NBI parameters is a natural trade-off between the beam costs and obtained performance. The neutral beams with lower energy are produced with much higher efficiency than those with higher energy, i.e., they are cheaper in power. However, their output in plasma in terms of current drive and neutron yield is essentially reduced, so the overall NBI efficiency is less when compared with more expensive higher energy beams.

The NB performance study reveals the following issues to be addressed in a neutral beam coupling with target plasma, which applies to any beam-driven tokamak:

- The NB production scheme depends on the injected energy range for efficient power transmission to plasma. The energy is consistent with the beam species mass, since

the beam penetration and capture by plasma are mainly governed by the beam particles velocity.

- The neutral beam power which can be injected to the tokamak is generally reduced not only by the injection port dimensions but also by the beam source current density and the accelerated beam angular dispersion. When the NB production scheme is chosen, the total beamline geometry needs to be optimized to deliver maximum power to plasma.
- The neutral beam direct losses in plasma include the shine-through power, which should be evaluated within the entire range of beam-plasma operation scenarios, including the cases with reduced plasma density and current drops.
- The initial beam losses in plasma also include the fast ion Larmor excursion beyond plasma LCMS bound, as well as their probability to be captured to the trapped “mirror” orbits.
- The real beam shape, which includes the beam envelope dimensions and the internal angular distribution, essentially affects the beam footprint and resulting plasma response when compared to simplified beam geometries like “thin” and/or “parallel” beam models. The reduced beam models can be reasonably applied only to beam-driven tokamaks with an expected small contribution from NB to current drive and neutron generation.
- The beam contribution to neutron generation is highly sensitive to the plasma temperature due to the “hot tail” growth with temperature in fast ion energy distributions.
- While the beam driven current is known to be highly dependent on the plasma temperature and density, the fast ion current in low aspect tokamaks can be essentially reduced by the toroidal effects, which are expressed in higher initial fast ion losses and in the toroidal velocity variation (bouncing).
- For a multi-component neutral beam, a specific contribution of each beam fraction needs to be evaluated. Together with the beam actual shape, the beam species composition may reduce the expected NB efficiency down by approximately two times (as shown in FNS-ST case);
- The optimum beam parameters, when evaluated for different criteria, typically do not coincide. For example, in our FNS-ST study, the NB axis optimum tangential aiming for the current drive and for the neutron generation appeared to be located at the opposite sides from the plasma magnetic axis.

Author Contributions: Conceptualization, E.D.; Data curation, A.P.; Methodology, E.D.; Project administration, B.K.; Resources, A.S.; Software, E.D.; Supervision, B.K. and A.S.; Validation, A.P.; Visualization, E.D.; Writing—original draft, E.D.; Writing—review & editing, E.D. and A.P. All authors have read and agreed to the published version of the manuscript.

Funding: This work was partially supported by NRC Kurchatov Institute.

Institutional Review Board Statement: Not applicable.

Informed Consent Statement: Not applicable.

Data Availability Statement: Not applicable.

Acknowledgments: The work was partially supported by the National Research Center “Kurchatov Institute”. Software testing was performed using the computing resources of the federal collective usage center Complex for Simulation and Data Processing for Mega-science Facilities at NRC “Kurchatov Institute”, <http://ckp.nrcki.ru/> (accessed on 23 February 2022).

Conflicts of Interest: The authors declare no conflict of interest.

References

1. Kuteev, B.V.; Azizov, E.A.; Bykov, A.S.; Dnestrovsky, A.Y.; Dokuka, V.N.; Gladush, G.G.; Zhirkin, A.V. Steady state operation in compact tokamaks with copper coils. *Nucl. Fusion* **2011**, *51*, 073013. [[CrossRef](#)]
2. Goncharov, P.R.; Kuteev, B.V.; Golikov, A.A.; Lukash, V.E.; Khayrutdinov, R.R.; Shpansky Yu, S.; Gryaznevich, M.P. Comparison between neutron yields of classical and spherical tokamaks. *VANT Fusion Ser.* **2011**, *2*, 36–43.
3. Akers, R.J.; Bond, A.; Butterly, R.J.; Carolan, P.G.; Counsell, G.F.; Cunningham, G.; Zaitsev, F.S. Steady state operation of spherical tokamaks. *Nucl. Fusion* **2000**, *40*, 1223. [[CrossRef](#)]
4. Chernyshev, F.V.; Afanasyev, V.I.; Gusev, V.K.; Ivanov, A.E.; Kurskiv, G.S.; Melnik, A.D.; Tolstyakov, S.Y. Study of fast-ion losses in experiments on neutral beam injection on the Globus-M spherical tokamak. *Plasma Phys. Rep.* **2011**, *37*, 553–571. [[CrossRef](#)]
5. Kikuchi, M.; Lackner, K.; Tran, M.Q. *Fusion Physics*; IAEA: Vienna, Austria, 2012.
6. Wesson, J. *Tokamaks*, 4th ed.; Oxford University Press: Oxford, UK, 2011.
7. Oikawa, T.; Park, J.M.; Polevoi, A.R.; Schneider, M.; Giruzzi, G.; Murakami, M.; Tani, K.; Sips, A.C.C.; Kessel, C.; Houlberg, W.; et al. Benchmarking of neutral beam current drive codes as a basis for the integrated modeling for ITER. In Proceedings of the 22nd International Conference on Fusion Energy, Geneva, Switzerland, 13–18 October 2008.
8. Hobirk, J.; Oikawa, T.; Fujita, T.; Fukuda, T.; Günter, S.; Gruber, O.; Team, A.U. Off-axis neutral beam current drive experiments on ASDEX upgrade and JT-60U. In Proceedings of the 30th European Physical Society Conference on Plasma Physics and Controlled Fusion, St. Petersburg, Russian, 7–11 July 2003.
9. Heidbrink, W.W.; van Zeeland, M.A.; Grierson, B.A.; Muscatello, C.M.; Park, J.M.; Petty, C.C.; Zhu, Y.B. Initial measurements of the DIII-D off-axis neutral beams. *Nucl. Fusion* **2012**, *52*, 094005. [[CrossRef](#)]
10. Challis, C.D.; Cordey, J.G.; Hamnén, H.; Stubberfield, P.M.; Christiansen, J.P.; Lazzaro, E.; Thompson, E. Non-inductively driven currents in JET. *Nucl. Fusion* **1989**, *29*, 563. [[CrossRef](#)]
11. Weiland, M.; Bilato, R.; Dux, R.; Geiger, B.; Lebschy, A.; Felici, F.; Eurofusion MST1 Team. RABBIT: Real-time simulation of the NBI fast-ion Distribution. *Nucl. Fusion* **2018**, *58*, 082032. [[CrossRef](#)]
12. Pankin, A.; McCune, D.; Andre, R.; Bateman, G.; Kritz, A. The tokamak Monte Carlo fast ion module NUBEAM in the National Transport Code Collaboration library. *Comput. Phys. Commun.* **2004**, *159*, 157–184. [[CrossRef](#)]
13. Asunta, O.; Govenius, J.; Budny, R.; Gorelenkova, M.; Tardini, G.; Kurki-Suonio, T.; Sipilä, S. Modelling neutral beams in fusion devices: Beamlet-based model for fast particle simulations. *Comput. Phys. Commun.* **2015**, *188*, 33–46. [[CrossRef](#)]
14. Schneider, M.; Eriksson, L.G.; Jenkins, I.; Artaud, J.F.; Basiuk, V.; Imbeaux, F.; JET-EFDA contributors. Simulation of the neutral beam deposition within integrated tokamak modelling frameworks. *Nucl. Fusion* **2011**, *51*, 063019. [[CrossRef](#)]
15. Dlougach, E.D.; Panasenkov, A.A.; Kuteev, B.V.; Filimonova, E.A. Light beam model for neutral beam injection optimization. *VANT Fusion Ser.* **2021**, *44*, 63–79. [[CrossRef](#)]
16. BTR Code for Neutral Beam Design. Available online: <https://sites.google.com/view/btr-code/home> (accessed on 8 August 2022).
17. BTR Code Source Repository. Available online: <https://github.com/EDlougach/BTR> (accessed on 8 August 2022).
18. Dlougach, E.D. BTR code for NBI design and study. *VANT Fusion Ser.* **2021**, *44*, 68–79. [[CrossRef](#)]
19. *ITER Final Design Report DDD 5.3*; IAEA: Vienna, Austria, 2001.
20. Dlougach, E.D.; BTOR Software for Injected Beam Capture and Performance in Tokamak Plasma (Python). Certificate of Computer Code Registration No 2020612368, Record 20.02.2020, Russia. Available online: <https://www1.fips.ru/ofpsstorage/BULLETIN/PrEVM/2020/02/20/INDEX.HTM> (accessed on 15 August 2022).
21. Panasenkov, A.A.; Ananyev, S.S.; Dlougach, E.D.; Kuteev, B.V. Analysis of the setup and parameters of the FNS-ST tokamak fast atom injector. *VANT Fusion Ser.* **2021**, *44*, 86–99. [[CrossRef](#)]
22. Pereverzev, G.V.; Yushmanov, P.N. *ASTRA Automated System for Transport Analysis in a Tokamak*; Preprint Max-Planck-Institut für Plasmaphysik ID 282186; Max-Planck-Institut für Plasmaphysik: Garching, Germany, 2002.
23. Janev, R.K.; Boley, C.D.; Post, D.E. Penetration of energetic neutral beams into fusion plasmas. *Nucl. Fusion* **1989**, *29*, 2125. [[CrossRef](#)]
24. Okano, K. Beam Driven Tokamak Fusion Reactors. *J. Nucl. Sci. Tech.* **1990**, *27*, 689–699. [[CrossRef](#)]
25. Dlougach, E.D.; Panasenkov, A.A.; Kuteev, B.V.; Filimonova, E.A. Neutral beam current ratio in the neutron source FNS-ST. *VANT Fusion Ser.* **2021**, *44*, 100–106. [[CrossRef](#)]